

AD-A101 111

TETRA TECH INC PASADENA CA

F/6 20/4

SINGULAR PERTURBATION METHOD FOR SUPERCAVITATING PROPELLERS. (U)

N00014-80-C-0277

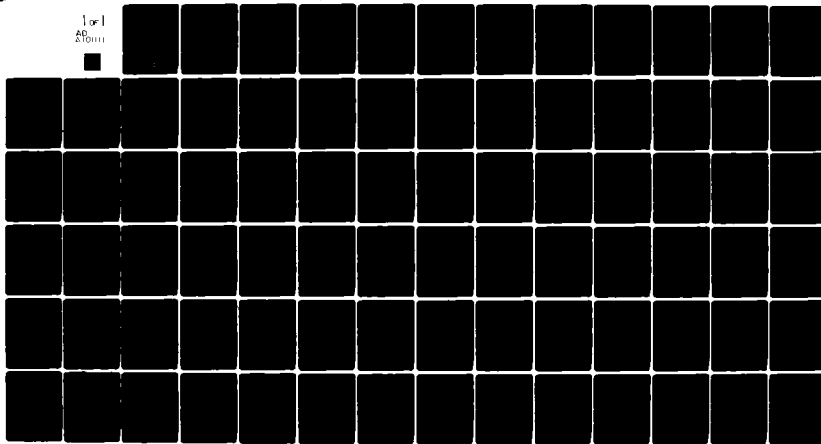
UNCLASSIFIED

JAN 81 O FURUYA

NL

TETRAT-TC-3369-01

1 of 1
AD-A101111



END
DATE
FILED
1-28-81
DTIC

END
DATE
FILED
7-81
DTIC

Report No. TC-3369-01
Contract No. N00014-80-C-0277

AD

SINGULAR PERTURBATION METHOD FOR
SUPERCAVITATING PROPELLERS

by

OKITSUGU FURUYA

DTIC FILE COPY
DTIC

TETRA TECH, INC.
630 NORTH ROSEMEAD BOULEVARD
PASADENA, CALIFORNIA 91107

JANUARY 1981

Prepared for

DAVID W. TAYLOR NAVAL SHIP R&D CENTER
BETHESDA, MARYLAND 20084

OFFICE OF NAVAL RESEARCH
800 NORTH QUINCY STREET
ARLINGTON, VIRGINIA 22217

Approved for public release;
distribution unlimited

ST 7 DTIC
ELECT JUL 8 1981
A

32746145

Report No. TC-3369-01
Contract No. N00014-80-C-0277

SINGULAR PERTURBATION METHOD FOR SUPERCAVITATING PROPELLERS

by
OKITSUGU FURUYA

TETRA TECH, INC.
630 NORTH ROSEMEAD BOULEVARD
PASADENA, CALIFORNIA 91107

JANUARY 1981

Prepared for

DAVID W. TAYLOR NAVAL SHIP R&D CENTER
BETHESDA, MARYLAND 20084

OFFICE OF NAVAL RESEARCH
800 NORTH QUINCY STREET
ARLINGTON, VIRGINIA 22217

Approved for public release;
distribution unlimited

Session For
SIS Serial
SIS TAB
SIS Log
SIS Logbook

UNCLASSIFIED

SECURITY CLASSIFICATION OF THIS PAGE (When Data Entered)

REPORT DOCUMENTATION PAGE		READ INSTRUCTIONS BEFORE COMPLETING FORM
1. REPORT NUMBER TC-3369-01	2. GOVT ACCESSION NO. AD-A101 111	3. RECIPIENT'S CATALOG NUMBER
4. TITLE (and Subtitle) SINGULAR PERTURBATION METHOD FOR SUPERCAVITATING PROPELLERS	5. TYPE OF REPORT & PERIOD COVERED Technical - Theory / Feb. 11, 1980 - Feb. 10, 1981	
7. AUTHOR(s) Okitsugu Furuya	6. PERFORMING ORG. REPORT NUMBER TC-3369-01	
8. CONTRACT OR GRANT NUMBER(s) N00014-80-C-0277	9. PERFORMING ORGANIZATION NAME AND ADDRESS TETRA TECH, INC. 630 North Rosemead Boulevard Pasadena, CA 91107	
10. CONTROLLING OFFICE NAME AND ADDRESS David W. Taylor Naval Ship R&D Center Department of the Navy Bethesda, MD 20084	11. PROGRAM ELEMENT, PROJECT, TASK AREA & WORK UNIT NUMBERS DWTNSRDC (1505) Req. #0192067 79ICT01	
12. REPORT DATE January 30, 1981	13. NUMBER OF PAGES 78	
14. MONITORING AGENCY NAME & ADDRESS (if different from Controlling Office) Office of Naval Research 800 North Quincy Street Arlington, VA 22217	15. SECURITY CLASS. (of this report) Unclassified	
16. DISTRIBUTION STATEMENT (of this Report) Approved for public release; distribution unlimited	17. DECLASSIFICATION/DOWNGRADING SCHEDULE	
18. DISTRIBUTION STATEMENT (of the abstract entered in Block 20, if different from Report)		
19. SUPPLEMENTARY NOTES Sponsored by the Naval Sea Systems Command General Hydrodynamic Research Program and administered by the David W. Taylor Naval Ship R&D Center, Code 1505, Bethesda, Maryland 20084.		
20. KEY WORDS (Continue on reverse side if necessary and identify by block number) supercavitating propeller singular perturbation method theory		
21. ABSTRACT (Continue on reverse side if necessary and identify by block number) The singular perturbation method for the supercavitating propeller had four scaling parameters; 1) span length R, 2) chord length c, 3) blade spacing d and 4) cavity length l_c . The first problem solved here assumed that c/R and l_c/R were of order ϵ but d/R was of order of unity. The nature of the singular perturbation problem for such a case was similar to that for the subcavitating propeller solved by Brockett except for the solution of the inner region. The thrust and torque coefficients were obtained explicitly without solving the integral equations. Since the non-linear supercavitating flow theory was employed in the present work as the inner		

UNCLASSIFIED

SECURITY CLASSIFICATION OF THIS PAGE (When Data Entered)

solution, there existed no limitation for the flow incidence angles or blade profile shapes and thus the present solution would provide more accurate results than those with the linearized theory.

The second problem treated here was the case in which c/R was of order of ϵ but λ_c/R and d/R were of order of unity. This was the case having long cavities behind the propeller blades so that even when the chord shrank to a line, the cavities were left behind the lifting lines. This portion of cavity sheets was called "source sheets", the singularity strengths of which were obtained through the cavity sheet matching, a totally different matching procedure from the regular matching. The first-order inner solution used a closure condition, i.e., the total source term S_0 equal to zero. As the result of the cavity sheet matching, however, it was discovered that the second-order inner solution had to use a finite S_0 , the value of which was determined through the matching. It seemed that the second-order matching automatically corrected the overstretching assumption made in the first-order inner solution.

Two other problems were posed, both having small blade spacings. The outer solutions may be quite different from those in the above two cases since if one looks at such a propeller from the far field, the blade elements will not be identified. This may require the actuator disc concept for the outer solution, with a conventional pressure jump across the disc if the cavity is short but with a cavity pressure drop to be applied if the cavity is long, similar to the theory of Tulin (1965). These two problems have not been carried out here due to the enormous amount of work required even for the first two problems.

UNCLASSIFIED

TABLE OF CONTENTS

	Page
LIST OF TABLES AND FIGURES	ii
ACKNOWLEDGMENT	iii
1.0 <u>BACKGROUND</u>	1
2.0 <u>BASIC THEORIES</u>	5
2.1 LINEARIZED SUPERCAVITATING PROPELLER THEORY	6
2.2 2-D NONLINEAR SUPERCAVITATING FOIL THEORY	11
2.3 2-D LINEARIZED SUPERCAVITATING FLOW THEORY.	16
3.0 <u>SINGULAR PERTURBATION METHOD FOR SUPERCAVITATING PROPELLERS</u>	21
3.1 SHORT CAVITY PROPELLER CASE (CASE 1)	24
3.1.1 <u>Outer Solution</u>	24
3.1.2 <u>Inner Solution</u>	32
3.1.3 <u>Matching Procedure</u>	37
3.1.4 <u>Propeller Performance</u>	44
3.2 LONG CAVITY PROPELLER CASE (CASE 2)	46
4.0 <u>CONCLUSION AND RECOMMENDATION</u>	57
<u>REFERENCES</u>	60
APPENDIX A	73

LIST OF TABLES AND FIGURES

ACKNOWLEDGMENT

This research was carried out under the Naval Sea Systems Command, General Hydromechanics Research Program, administered by the David Taylor Naval Ship Research and Development Center, Contract N00014-80-C-0277.

Solving the propeller flow problem is inherently difficult due to its geometric complexity as well as the propeller rotational motion. For fully wetted propellers, many different types of theories have been developed to date, both for design and off-design analyses. These include lifting line and lifting surface theories, using the singularity distribution method. In the performance prediction method the strengths of sources and vortices represent the thickness and loading of blade, respectively and are to be determined by satisfying the flow-tangency condition on the propeller blade surface. The numerical analysis using high speed computer is essential and sometimes encounters the instability problem.

The problem of supercavitating (s/c) propeller flow is even more difficult due to the additional feature, i.e., the existence of the cavity on the suction side of the blade. The extent of cavity varies significantly, depending upon the ship speed and/or propeller rotational speed. At the design point, the supercavitating propeller usually operates with relatively short to medium length cavities. However, as the flow speed or rotational speed increases, the cavity becomes longer with increase in thickness. The flow passage between blades is gradually blocked and finally totally choked over the entire blade span. Although the effect of the thick cavity may theoretically be represented by the source distribution, a difficult problem exists in that the location of the cavity is not known until the complete supercavitating propeller flow is solved.

Three different types of concepts exist in accounting for this thick and long cavity effect on the s/c propeller flow. When the sectional loading used for propeller analysis is calculated based on the single foil configuration, the 'retarding' flow correction due to the cavity blocking by Tulin (1965) may be necessary in addition to the conventional induced flow correction.

This concept is similar to that of the actuator disk theory, except that the cavity pressure instead of fully recovered pressure at downstream infinity is used in the momentum theory. The effective incoming flow velocity, different from that of the upstream infinity, is used as part of the correction to the propeller flow diagram. This method was actually applied to the recent Hydronautics design of a supercavitating propeller, designated as Model 7607.02 (see the report by Bohn and Altman (1976)). Experimental results for the propeller obtained by Bohn (1977) and Peck (1977) showed that the design method overpredicted the thrust by about 10 percent.

Instead of correcting the effective incoming flow with the retarding flow effect, the second category of the concept utilizes the forces calculated from the cascade flow analysis for the propeller sectional loading. This type of method is widely used in the design and analysis for the pump and turbine in which the flow is usually well confined in the circular duct. The force coefficients obtained in this theory are generally much lower than those of single foil cases because the pressure on the blade is substantially lowered by the cavity attached to the adjacent blade. These forces are now used for the induced flow corrections due to the free vortex sheet. It must be noted that the retarding flow correction is not necessary because it is considered that the cavity blockage effect is already taken care of when obtaining the sectional forces. The author recently developed such a theory based on the above concept (see Furuya (1976, 1978)). The prediction capability of the theory is good for low advance speed range J where a strong cavity choking condition prevails. Incidentally, an accurate prediction of the s/c propeller performance at low J 's is important since the high speed taking-off condition occurs under such conditions. However, for larger J 's for which the cavity has a shorter length, the theory substantially deviates from the experimental data. It means that the supercavitating propeller theory based on the cascade data will be

suitable for predicting the off-design performance at the same as or lower J than J_d of design point but that the accuracy for larger J 's is questionable.

One of the major questions arising from applying the two-dimensional cascade flow to the three-dimensional propeller flow is as to what flow incidence angle must be used for determining the force. Since in the cascade flow, unlike the single foil flow case, the flow field is completely separated by the cascade blade, there exist two reference flow angles, one at upstream infinity and the other at downstream infinity. In the pump and turbine flow analysis it is conventional to use the geometric mean flow angle. This may be understandable since in such devices the upstream flow field is physically separated from the downstream flow field. In the propeller flow the flow field is so called "singly" connected like the single foil case. The only difference is that the cascade effect locally exists in the former. It is, therefore, not quite clear which angle is to be used for the present propeller analysis, the upstream flow angle or geometric mean flow angle of cascade theory. The above propeller theory of Furuya (1978) used the former for the two-dimensional cascade flow analysis. It is considered that an appropriate flow angle to be used may be somewhere in between the above two extreme cases.

The third category is that of Yim (1978) who developed a design method by combining the lifting surface theory with cavity effects. The strength of source as well as that of doublet is determined by satisfying the boundary conditions both on the solid and cavity boundaries. However, the method was developed as a design tool, not applicable to the off-design performance prediction of supercavitating propellers.

In the situation just described, it is considered useful to investigate the problem from a different point of view, namely, with the singular perturbation method (SPM). Brockett (1972)

first applied the method to the subcavitating propeller flow. He used the linearized propeller theory for the "outer" solution and a two-dimensional linearized theory of the fully wetted single foil flow for the "inner" solution. Through the matching procedure the circulation distribution of the outer solution was explicitly determined with the induced flow corrections included. However, the scaling parameters used in the work of Brockett were limited to two, i.e., chord and span lengths, just like the finite span wing case, so that the blade aspect ratio ϵ was only the small parameter for expansions to be made. It means that the results of Brockett can only be applied to such propellers having large aspect ratio with small number of blades, e.g., two to three.

The singular perturbation problem for the supercavitating propeller is much more complex in that there exist four scaling parameters. These include 1) span length, 2) chord length, 3) blade spacing and 4) cavity length. Although the blade spacing must have been included even in the SPM of Brockett (1972) for the conventional propeller, it was just omitted there under the condition that the propeller blades be sparsely distributed as mentioned above. Different combinations of the above four parameters will provide various types of problems for the supercavitating propeller with SPM. In the present study four most typical cases are identified, as will be seen in Section 3 and the solution methods for the first two problems among others will be presented herein.

We will start with the basic theories which will form the basis for the inner and outer solutions (Section 2), which will be followed by the classification of the problem (Section 3) and then its solution methods.

The singular perturbation method for supercavitating propellers will employ various two- and three-dimensional flow theories as inner and outer solutions. Most of these theories have been well established and will be found much in literature. One should study, however, on which theory is suitable for the inner or outer solution and for the matching procedure. As a preparatory work for the major part of the present study, the basic two- and three-dimensional theories to be used herein will be described in the following.

2.1 LINEARIZED SUPERCAVITATING PROPELLER THEORY

There exist various ways of deriving the potential function ϕ for propeller flows but only a limited number of papers are available for the supercavitating propeller flow. The paper by Cox (1968) represents such a theory and this method will be employed throughout the present work as the outer solution.

Figure 2.1.1 shows a schematic diagram of a supercavitating propeller blade rotating around the x -axis in the uniform flow of velocity U approaching from the negative infinity of x . The center of the propeller shaft is placed along the x -axis. Although the cylindrical coordinate system (x, r, θ) will be used in the present propeller analysis, it will be transferred, if necessary, into the cartesian coordinate system shown in Figure 2.1.1. The velocity components in the x, r, θ directions are first written in terms of the perturbation quantities for U as $(U + u_x, u_r, u_{\theta 0})$ where the subscript 0 is used for the inertial coordinate θ in order to distinguish it from the rotating coordinate. Defining \underline{u} as $(u_x, u_r, u_{\theta 0})$, the linearized equation of motion can be written

$$\frac{\partial \underline{u}}{\partial t} + U \frac{\partial \underline{u}}{\partial x} = - \nabla \frac{\hat{p}}{\rho},$$

which will be expressed in terms of the velocity potential ϕ as follows

$$\frac{\partial \phi}{\partial t} + U \frac{\partial \phi}{\partial x} = - \hat{p} \quad (2.1.1)$$

where

$$\underline{u} = \nabla \phi \quad (2.1.2)$$

$$\hat{p} = p/\rho.$$

Solution for the partial differential equation (2.1.1) is obtained

$$\hat{p}(x, r, \theta_0; t) = -\frac{1}{U} \int_{-\infty}^{x-x'} \hat{p}\left(v+x', r, \theta_0; t - \frac{x-(v+x')}{U}\right) dv \quad (2.1.3)$$

where the boundary condition of $\hat{p} = 0$ at $x = -\infty$ has been used. Applying the continuity equation $\underline{\nabla} \cdot \underline{u} = 0$ to Equations (2.1.1) and (2.1.2), the Laplace equation is obtained for \hat{p}

$$\nabla^2 \hat{p} = 0. \quad (2.1.4)$$

Use of the Green's identity for \hat{p} will provide

$$\begin{aligned} \hat{p}(x, r, \theta_0; t) &= -\frac{1}{4\pi} \sum_{k=1}^K \left\{ \iint_{S_b} \hat{p}(x', r', \theta'; t) \frac{\partial}{\partial n_0} \left(\frac{1}{R_{\psi_0}} \right) ds \right. \\ &\quad \left. - \iint_{S_b+S_c} \frac{1}{R_{\psi_0}} \frac{\partial}{\partial n_0} \left[\hat{p}(x', r', \theta'; t) \right] ds \right\} \quad (2.1.5) \end{aligned}$$

where

\underline{n} = normal to linearized surface, positive from pressure side to suction side

$$R_{\psi_0} = \left[(x - x')^2 + r'^2 + r^2 - 2r'r \cos \psi_0 \right]^{\frac{1}{2}}$$

$$\dot{\psi}_0 = \dot{\psi}'_0 - \dot{\psi}_0 + \sigma_k$$

$$\dot{\psi}'_0 = \dot{\psi}' - \omega t$$

$$\sigma_k = \frac{2\pi}{K} (k - 1)$$

K = number of blades

S = moving surface consisting of propeller blade surface S_b and cavity surface S_c

S_b, S_c = propeller blade and cavity surfaces, respectively.

The moving blade surface S is considered to be composed of helical lines having varying pitch in the r -direction; i.e.,

$$S: x - \theta R \lambda(r) = 0$$

$$\lambda(r) = U(r)/\omega R$$

where λ denotes the advance coefficient as a function of r .
The directional derivative for this surface is then given

$$\frac{\partial}{\partial n_0} = - \frac{r \frac{\partial}{\partial x} - r(\theta'_0 + \omega t) R \lambda_r \frac{\partial}{\partial r} - \frac{R \lambda}{r} \frac{\partial}{\partial \theta'_0}}{\left[r^2 + (R \lambda)^2 + (r \theta'_0 R \lambda_r)^2 \right]^{\frac{1}{2}}}$$

where $\lambda_r = d\lambda/dr$. Thus,

$$\frac{\partial}{\partial n_0} \frac{1}{R \phi'_0} = - \frac{r(x - x') + R \lambda r \sin \theta'_0 - r(\theta'_0 + \omega t) R \lambda_r (r' - r \cos \theta'_0)}{\left[r^2 + (R \lambda)^2 + \{r(\theta'_0 + \omega t) R \lambda\}^2 \right]^{\frac{1}{2}} R^3 \phi'_0},$$

and

$$ds = \left[r^2 + (R \lambda)^2 + \{r(\theta'_0 + \omega t) R \lambda_r\}^2 \right]^{\frac{1}{2}} d\theta dr.$$

For the steady state problem presently investigated, time t is set to zero in the above equations. It means that the rotating axis and inertial axis coincide instantaneously, then

$$\phi(x, r, \theta) \equiv \phi_V + \phi_S$$

where

ϕ_V = potential due to the vortex

$$= - \frac{1}{2} \sum_{k=1}^K \int_{r_h}^1 \int_{\theta_L}^{\theta_T} \Delta \hat{p}(r', \theta') \left[\int_{-\infty}^{x - \theta' \lambda} \frac{N_V}{R_V^3} dv \right] d\theta' dr', \quad (2.1.6)$$

ϕ_S = potential due to the source

$$= - \frac{1}{2} \sum_{k=1}^K \int_{r_h}^1 \int_{\theta_L}^{\theta_E} s_p(r', \theta') \left[\int_{\infty}^{x - \theta' \lambda} \frac{dv}{R_V^2} \right]^{\frac{1}{2}} d\theta' dr' \quad (2.1.7)$$

r_h = radial coordinate corresponding to the propeller hub

θ_L , θ_T , θ_E = angular coordinates at the blade leading edge, trailing edge, and at the cavity end point, respectively

$$\Delta p = p^+ - p^- \text{ (pressure doublet)}$$

$$s_p = \frac{\partial p^+}{\partial n} - \frac{\partial p^-}{\partial n} \text{ (pressure source)}$$

$$M = r'^2 + \lambda^2 + (r' \theta' \lambda_r)^2$$

$$N_v = r'v + r\lambda \sin \tilde{\phi} - \frac{r}{\lambda} (v - x)v_r (r' - r \cos \tilde{\phi})$$

$$\tilde{\phi} = -\frac{1}{\lambda} (v - x) - \theta + \sigma_k$$

$$R_v = \left[v^2 + r'^2 + r^2 - 2r'r \cos \tilde{\phi} \right]^{\frac{1}{2}}$$

v = dummy variable for integrals.

It must be mentioned also that the normalization has been made for all quantities above as follows,

$$(\bar{x}, \bar{r}, \bar{x}', \bar{r}', \bar{v}) \equiv (x, r, x', r', v')/R$$

$$\bar{\phi} = \phi/RU$$

$$\bar{N}_v = N_v/R^2$$

$$\bar{R}_v = R_v/R$$

$$\bar{\lambda}_r = \lambda/R$$

$$\bar{s}_p = s_p/2\pi U^2/R$$

$$\bar{\Delta p} = \Delta p/2\pi U^2$$

where R is the propeller radius. After normalization, the bar above each character has been deleted. Therefore, it should be understood that all mathematical expressions in equations hereafter, including Equations (2.1.6) and (2.1.7), are those which were normalized.

The potential ϕ due to the source effect in Equation (2.1.7) is rather complex. A simpler form can be obtained if the source

distribution is used instead of the pressure source s_p ,

$$\phi_s = -\frac{1}{2} \sum_{k=1}^K \int_{r_h}^1 \int_{\hat{\theta}_L}^{\hat{\theta}_E} \frac{s(r', \theta') d\theta' dr'}{R_{\theta'}}, \quad (2.1.8)$$

where

$$R_{\theta'} = \left[(x - \theta')^2 + r'^2 + r^2 - 2r'r \cos \hat{\theta}_{\theta'} \right]^{\frac{1}{2}}$$

$$\hat{\theta}_{\theta'} = \theta' - \theta + \sigma_k.$$

In Equation (2.1.8), $s(r', \theta')$ is the source term (not a pressure source in this case) which represents the blade and cavity thickness.

2.2 2-D NONLINEAR SUPERCAVITATING FOIL THEORY

In order to provide a high accuracy of the results obtained from the present SPM, a nonlinear theory for the supercavitating (s/c) foil will be used as an inner solution. Many flow models having various cavity closure conditions are available. These include the open wake model of Wu (1962), and single and double spiral vortex models of Tulin (1964). Among others, the single spiral vortex model of Tulin will be used, the reason for this selection being explained later.

The single spiral vortex model was first employed by Larock and Street (1965, 1968) in the nonlinear theory, but only applied for the calculation of the s/c flat-plate foil characteristics and for the inverse specification of foil profile. The theory and computer program were recently developed for general profile cases by Furuya and Maekawa (1980) and compared with experimental data. The key features of the theory necessary for the singular perturbation method will be summarized here. The flow configuration and boundary conditions are shown in Figure 2.2.1(a) in which the physical coordinate system employs (\bar{x}, \bar{y}) in tune with that used in the inner region as will be seen later. The physical flow field is mapped onto the potential plane W as shown in Figure 2.2.1(b) which is then transformed onto the upper half of a new plane $\zeta = \xi + i\eta$ of Figure 2.2.1(c) by a mapping function

$$\zeta = a \sqrt{\frac{W}{\phi_l - W}} \quad (2.2.1)$$

or

$$W = \frac{\phi_l \zeta^2}{a^2 + \zeta^2}. \quad (2.2.2)$$

The cavity end point is mapped to infinity and the infinity point in $\bar{y} = \bar{x} + i\bar{y}$ or W plane is now mapped onto a point $\zeta = ia$. A hodograph variable ω is introduced

$$\frac{dW}{d\bar{\gamma}} = q e^{-i\theta} = q_c e^{-i\omega} \quad (2.2.3)$$

where q and θ are the magnitude and direction of the flow velocity. Thus

$$\omega = \theta + i\tau, \quad \tau = \ln \left(\frac{q}{q_c} \right),$$

and

$$q_c = \sqrt{1 + \sigma} q_1, \quad \sigma = \frac{p_1 - p_c}{\frac{1}{2} \rho q_1^2}$$

where q_1 and q_c denote the uniform flow velocity at the upstream infinity and that on the cavity wall, respectively.

The boundary conditions on the real-axis ξ are now expressed either in terms of θ or τ ;

- (i) $\tau = 0, \quad -\infty < \xi < -1$ and $b < \xi < \infty$,
- (ii) $\theta = \beta, \quad -1 < \xi < 0, \quad \beta = \tan^{-1} \{dy(x)/dx\}$
- (iii) $\theta = \pi + \beta, \quad 0 < \xi <$

where $y(x)$ denotes the foil profile shape of the wetted portion. This is a typical mixed-type boundary value problem, and the solution for ω is readily written

$$\omega(\xi) = \sqrt{(\xi + 1)(\xi - b)} \left\{ \begin{aligned} & \frac{1}{2\pi i} \int_{-1}^b \frac{2\beta}{i\sqrt{(1 + \xi')(b - \xi')}} \frac{d\xi'}{\xi' - \xi} \\ & + \frac{1}{2\pi i} \int_0^b \frac{2\pi}{i\sqrt{(1 + \xi')(b - \xi')}} \frac{d\xi'}{\xi' - \xi} + P \end{aligned} \right\}. \quad (2.2.4)$$

We have a total of four unknown quantities, a , b , P , ϕ_L , requiring four equations to determine them uniquely.

The various boundary conditions will be applied;

(i) at infinity

$$\omega(ia) = i \ln \left(\frac{1}{\sqrt{1+\sigma}} \right) : \quad 2 \text{ equations}$$

(ii) length of arc = \tilde{S} arc: 1 equation

(iii) body-cavity system closure condition (see Larock and Street (1965)),

$$\operatorname{Re} \left\{ \oint_C \omega dW \right\} = 0: \quad 1 \text{ equation,}$$

or

$$\operatorname{Re} \left\{ \frac{d\omega(\zeta)}{d\zeta} \Big|_{\zeta=ia} \right\} = 0.$$

The report of Furuya and Maekawa (1980) describes the method of solving the above system of nonlinear integral equations for the four solution parameters in detail.

It must be pointed out here that not all of the nonlinear theories quoted before are applicable to the inner solution of the problem. We should exclude those theories whose body-cavity systems do not close in the potential plane W . This point will become clearer if $W(\tilde{\gamma})$ is expanded as $\tilde{\gamma} \rightarrow \infty$. Let's use the double-spiral vortex model as an example, the flow configuration of which is shown in Figure 2.2.2(a). Mapping the potential plane $W = \tilde{\gamma} + i\tilde{\zeta}$ onto the upper half of the ζ -plane, the hodograph solution ω can be obtained as

$$\omega(\zeta) = \sqrt{(\zeta+1)(\zeta-b)} \left\{ -\frac{1}{\pi} \int_{-1}^b \frac{\zeta}{i\sqrt{(1+\zeta')(b-\zeta')}} \frac{d\zeta'}{\zeta' - \zeta} - \right.$$

$$\begin{aligned}
& - \int_{-1}^b \frac{1}{\sqrt{(1+\xi')(b-\xi')}} \frac{d\xi'}{\xi' - \zeta} \\
& + \frac{\ln \sqrt{1+\zeta}}{\pi} \left[\int_b^d \frac{1}{\sqrt{(\xi'+1)(\xi'-b)}} \frac{d\xi'}{\xi' - \zeta} - \int_c^{-1} \frac{1}{\sqrt{(\xi'+1)(\xi'-b)}} \frac{d\xi'}{\xi' - \zeta} \right] \}
\end{aligned} \tag{2.2.5}$$

where

$$\frac{dW}{d\bar{Y}} = q e^{-i\theta} = q_1 e^{-i\omega}, \tag{2.2.6}$$

thus

$$\omega = \theta + i \ln q/q_1.$$

$$W = A\zeta^2; A = \text{solution parameter, yet to be known.}$$

From Equation (2.2.6),

$$d\bar{Y} = \frac{1}{q_1} e^{i\omega} \frac{dW}{d\zeta} d\zeta,$$

or

$$d\bar{Y} \sim \frac{1}{q_1} e^{i\omega(\infty)} \left[1 + i\omega'(\infty) \frac{1}{\zeta} + \frac{i\omega''(\infty) - \omega'(\infty)^2}{2} \frac{1}{\zeta^2} + \dots \right] \cdot 2A\zeta d\zeta$$

as $\zeta \rightarrow \infty$.

(2.2.7)

Integration of both sides of Equation (2.2.7) provides

$$\bar{Y} \sim AK_0 (\zeta^2 + 2K_1 \zeta + 2K_2 \ln \zeta + \dots), \text{ as } \zeta \rightarrow \infty \tag{2.2.8}$$

where

$$K_0 = e^{i\omega(\infty)}/q_1$$

$$K_1 = i\omega'(\infty)$$

$$K_2 = \left\{ i\omega''(\infty) - \omega'(\infty)^2 \right\} / 2.$$

Inverting Equation (2.2.7), one obtains

$$w = A\zeta^2 \sim \frac{\bar{\gamma}}{K_0} - 2K_1 \sqrt{\frac{A\bar{\gamma}}{K_0}} - AK_2 \ln \bar{\gamma} + \dots, \text{ as } z \rightarrow \infty.$$

The first, second and third terms in expansion represent the uniform flow, corner flow and source-circulation flows, respectively. Each term, except for the second one, can possibly find its counterpart from the outer solution. However, the second item, i.e., corner flow part, cannot be matched with the outer solution. This illustrates the difficulty of using any flow model which does not close in the downstream infinity, particularly in the potential plane. Note the difference of the potential planes in Figure 2.2.1(b) and Figure 2.2.2(b); one is closed and the other is open. It is for this reason that we have chosen a single spiral vortex model for the inner solution.

2.3

2-D LINEARIZED SUPERCAVITATING FLOW THEORY

We will utilize the results of the nonlinear theory as the inner solution for the singular perturbation method. As will be seen later, however, a linearized theory is necessary for conveniently determining the source strength on the body-cavity system. The most suitable linearized theory for determining such source strength is that of the singularity distribution method. Since the first introduction of the method by Tulin (1953), many researchers presented papers for various types of problems. However, the basic concept is described in the original paper by Tulin for the drag body case and in that of Fahner and Spiegel (1966) for the lifting body case. The linearized flow configuration is shown in Figure 2.3.1 and the linearized boundary conditions for the perturbed velocities u and v are given as follows:

$$\begin{aligned} u^+ &= \frac{\sigma}{2} \cdot q_1 \quad , \quad 0 < \bar{x} < 1, \bar{y} = 0^+, \\ u^- &= \frac{\sigma}{2} \cdot q_1 \quad , \quad 1 < \bar{x} < \lambda_c, \bar{y} = 0^-, \\ v^- &= q_1 \cdot f'(\bar{x}) \quad , \quad 0 < \bar{x} < 1, \bar{y} = \bar{0}, \end{aligned}$$

where

$$\sigma = \frac{p_1 - p_c}{\frac{1}{2} \rho q_1^2}.$$

If the source $s_1(\bar{x})$ ($0 < \bar{x} < 1$), $s_2(\bar{x})$ ($1 < \bar{x} < \lambda_c$) and dipole $\gamma(\bar{x})$ are distributed along the slit shown in Figure 2.3.1, i.e., for $0 < \bar{x} < \lambda_c$, the induced velocities due to these singularities will be given

$$u^+ = u^- = \frac{1}{2\pi} \int_0^1 \frac{s_1(\bar{x}')}{\bar{x} - \bar{x}'} d\bar{x}' \quad , \quad 0 < \bar{x} < 1 \quad (2.3.1)$$

$$u^+ = u^- = \frac{1}{2\pi} \int_1^{\lambda_c} \frac{s_2(\bar{x}')}{\bar{x} - \bar{x}'} d\bar{x}' \quad , \quad 1 < \bar{x} < \lambda_c \quad (2.3.2)$$

$$v^+ = \frac{s_1(\bar{x})}{2}, \quad v^- = -\frac{s_1(\bar{x})}{2}, \quad 0 < \bar{x} < 1 \quad (2.3.3)$$

$$v^+ = \frac{s_2(\bar{x})}{2}, \quad v^- = -\frac{s_2(\bar{x})}{2}, \quad 1 < \bar{x} < \zeta_c \quad (2.3.4)$$

$$u^+ = \frac{\gamma(\bar{x})}{2}, \quad u^- = -\frac{\gamma(\bar{x})}{2}, \quad 0 < \bar{x} < 1 \quad (2.3.5)$$

$$v^+ = v^- = -\frac{1}{2\pi} \int_0^L \frac{\gamma(\bar{x}')}{\bar{x} - \bar{x}'} d\bar{x}', \quad 0 < x < 1. \quad (2.3.6)$$

The boundary conditions on the slit are therefore satisfied by combining Equations (2.3.1) to (2.3.6), providing a system of integral equations with respect to $s_1(\bar{x})$, $s_2(\bar{x})$ and $\gamma(\bar{x})$,

$$\frac{1}{2\pi} \int_0^1 \frac{s_1(\bar{x}')}{\bar{x} - \bar{x}'} d\bar{x}' + \frac{1}{2\pi} \int_1^{\zeta_c} \frac{s_2(\bar{x}')}{\bar{x} - \bar{x}'} d\bar{x}' + \frac{\gamma(\bar{x})}{2} = \frac{\sigma}{2} q_1, \quad 0 < \bar{x} < 1 \quad (2.3.7)$$

$$\frac{1}{2\pi} \int_0^1 \frac{s_1(\bar{x}')}{\bar{x} - \bar{x}'} d\bar{x}' + \frac{1}{2\pi} \int_1^{\zeta_c} \frac{s_2(\bar{x}')}{\bar{x} - \bar{x}'} d\bar{x}' = \frac{\sigma}{2} q_1, \quad 1 < \bar{x} < \zeta_c \quad (2.3.8)$$

$$-\frac{1}{2\pi} \int_0^1 \frac{\gamma(\bar{x}')}{\bar{x} - \bar{x}'} d\bar{x}' - \frac{s_1(\bar{x})}{2} = q_1 \cdot f'(\bar{x}), \quad 0 < \bar{x} < 1. \quad (2.3.9)$$

Applying the inversion formula given in Appendix A to Equation (2.3.8), the following result will be obtained

$$s_2(\bar{x}) = \left(\frac{\bar{x} - 1}{\zeta_c - \bar{x}} \right)^{\frac{1}{2}} \left\{ -\frac{\sigma}{2} q_1 + \frac{1}{\pi} \int_0^1 \left(\frac{\zeta_c - \bar{x}'}{1 - \bar{x}'} \right)^{\frac{1}{2}} \frac{s_1(\bar{x}')}{\bar{x} - \bar{x}'} d\bar{x}' \right\} \quad (2.3.10)$$

where a singularity at $\bar{x} = \zeta_c$ has been placed for representing an abrupt termination of the cavity. $s_2(\bar{x})$ is now substituted into Equation (2.3.7),

$$\frac{1}{\pi} \int_0^1 \left(\frac{i_c - \bar{x}'}{1 - \bar{x}'} \right)^{\frac{1}{2}} \frac{s_1(\bar{x}')}{\bar{x} - \bar{x}'} d\bar{x}' = \beta q_1 - \gamma(\bar{x}) \left(\frac{i_c - \bar{x}}{1 - \bar{x}} \right)^{\frac{1}{2}}. \quad (2.3.11)$$

Application of the inversion formula again to Equation (2.3.11) yields an expression for $s_1(\bar{x})$ in terms of $\gamma(\bar{x})$;

$$s_1(\bar{x}) = \left(\frac{\bar{x}}{i_c - \bar{x}} \right)^{\frac{1}{2}} \left\{ -\beta q_1 + \frac{1}{\pi} \int_0^1 \left(\frac{\bar{x}'}{i_c - \bar{x}'} \right)^{\frac{1}{2}} \gamma(\bar{x}') \frac{d\bar{x}'}{\bar{x} - \bar{x}'} \right\} \quad (2.3.12)$$

Substitution of $s_1(\bar{x})$ in Equation (2.3.12) into Equation (2.3.9) eliminates $s_1(\bar{x})$, and results in the following integral equation for $\gamma(\bar{x})$ only;

$$\begin{aligned} & \frac{1}{2\pi} \int_0^1 \left\{ \left(\frac{i_c - \bar{x}}{\bar{x}} \right)^{\frac{1}{2}} + \left(\frac{i_c - \bar{x}'}{\bar{x}'} \right)^{\frac{1}{2}} \right\} \frac{\gamma(\bar{x}')}{\bar{x} - \bar{x}'} d\bar{x}' \\ &= \frac{\beta}{2} q_1 - \left(\frac{i_c - \bar{x}}{\bar{x}} \right)^{\frac{1}{2}} f'(\bar{x}) \cdot q_1. \end{aligned} \quad (2.3.13)$$

Change of variable with

$$\kappa = \left(\frac{\bar{x}}{i_c - \bar{x}} \right)^{\frac{1}{2}}, \quad \kappa' = \left(\frac{\bar{x}'}{i_c - \bar{x}'} \right)^{\frac{1}{2}} \quad (2.3.14)$$

will transform Equation (2.3.13) into the following form

$$\frac{1}{\pi} \int_0^e \frac{\gamma(\bar{x}'(\kappa'))}{(1 + \kappa'^2)} \frac{d\kappa'}{\kappa - \kappa'} = \frac{q_1}{1 + \kappa^2} \left\{ \beta \kappa - f'(\bar{x}(\kappa)) \right\} \quad 0 < \kappa < e \quad (2.3.15)$$

where

$$\begin{aligned} \bar{x}(\kappa) &= \frac{i_c \kappa^2}{1 + \kappa^2}, \quad \bar{x}'(\kappa') = \frac{i_c \kappa'^2}{1 + \kappa'^2} \\ e &= 1 / (i_c - 1)^{\frac{1}{2}}. \end{aligned} \quad (2.3.16)$$

Finally, the dipole distribution of $\gamma(\bar{x})$ is obtained by inverting Equation (2.3.15);

$$\begin{aligned}\gamma(\bar{x}(\kappa)) &= \frac{\sigma}{2} q_1 (\cos \beta)^{\frac{1}{2}} \left(\frac{e - \kappa}{\kappa} \right)^{\frac{1}{2}} \left(\sin \frac{\beta}{2} + \kappa \cos \frac{\beta}{2} \right) \\ &+ \frac{q_1}{\pi} \left(1 + \kappa^2 \right) \left(\frac{e - \kappa}{\kappa} \right)^{\frac{1}{2}} \int_0^e \left(\frac{\kappa'}{e - \kappa'} \right)^{\frac{1}{2}} \frac{f'(\bar{x}'(\kappa'))}{1 + \kappa'^2} \frac{d\kappa'}{\kappa - \kappa'}, \quad 0 < \kappa < e\end{aligned}\quad (2.3.17)$$

where

$$\beta = \tan^{-1}(e)$$

and the leading edge singularity has been introduced above for representing the stagnation flow within the framework of linearized theory.

$s_1(\bar{x})$ and $s_2(\bar{x})$ will then be calculated by substituting Equation (2.3.17) into (2.3.12), followed by (2.3.12) into (2.3.10)

$$\begin{aligned}s_1(\bar{x}(\kappa)) &= \frac{\sigma}{2} q_1 (\cos \beta)^{\frac{1}{2}} \left(\frac{\kappa + e}{\kappa} \right)^{\frac{1}{2}} \left(\sin \frac{\beta}{2} - \kappa \cos \frac{\beta}{2} \right) \\ &- \frac{q_1}{\pi} (1 + \kappa^2) \left(\frac{\kappa + e}{\kappa} \right)^{\frac{1}{2}} \int_0^e \left(\frac{\kappa'}{e - \kappa'} \right)^{\frac{1}{2}} \frac{f'(\bar{x}'(\kappa'))}{1 + \kappa'^2} \frac{d\kappa'}{\kappa + \kappa'} \\ &- q_1 f'(\bar{x}(\kappa))\end{aligned}\quad (2.3.18)$$

and

$$\begin{aligned}s_2(\bar{x}(\kappa)) &= \frac{\beta}{2} q_1 (\cos \beta)^{\frac{1}{2}} \left[\left\{ \left(\frac{\kappa + e}{\kappa} \right)^{\frac{1}{2}} - \left(\frac{\kappa - e}{\kappa} \right)^{\frac{1}{2}} \right\} \sin \frac{\beta}{2} \right. \\ &\quad \left. - \kappa \left\{ \left(\frac{\kappa + e}{\kappa} \right)^{\frac{1}{2}} + \left(\frac{\kappa - e}{\kappa} \right)^{\frac{1}{2}} \right\} \cos \frac{\beta}{2} \right]\end{aligned}$$

$$\begin{aligned}
& - \frac{q_1}{\pi} (1 + \kappa^2) \left[\left(\frac{\kappa + e}{\kappa} \right)^{\frac{1}{2}} \int_0^e \left(\frac{\kappa'}{e - \kappa'} \right)^{\frac{1}{2}} \frac{f'(\bar{x}'(\kappa'))}{1 + \kappa'^2} \frac{d\kappa'}{\kappa + \kappa'} \right. \\
& \left. + \left(\frac{\kappa - e}{\kappa} \right) \int_0^e \left(\frac{\kappa'}{e - \kappa'} \right)^{\frac{1}{2}} \frac{f'(\bar{x}'(\kappa'))}{1 + \kappa'^2} \frac{d\kappa'}{\kappa - \kappa'} \right]. \tag{2.3.19}
\end{aligned}$$

The yet unknown parameter, i.e., length of cavity λ_c in these equations, can be determined by the cavity closure condition,

$$\int_0^1 s_1(\bar{x}') d\bar{x}' + \int_1^{\lambda_c} s_2(\bar{x}') d\bar{x}' = 0. \tag{2.3.20}$$

Application of the singular perturbation method to the supercavitating propeller flow will lead to multiple problems. Most of the hydrodynamic problems solved with this method have only two characteristic lengths in the flow field. Three-dimensional fully wetted and cavitating single foil flows were solved by many researchers including Van Dyke (1964), Shen and Ogilvie (1972), Leehey (1973), Furuya (1975) and James (1975). The two characteristic scales for such flows were chord and span lengths with its ratio assumed to be small. The problem of thin foils with rounded leading edges was also treated with the singular perturbation method, for the fully wetted flow by Van Dyke (1964) and for the supercavitating flow by Furuya and Acosta (1973). Again, two characteristic lengths, i.e., chord and leading edge radius, existed.

For the supercavitating propeller flow, however, we have four characteristic lengths. These are

- i) propeller radius (R),
- ii) blade chord length (c),
- iii) cavity length (ℓ_c), and
- iv) propeller blade spacing (d).

With these four physical parameters, many combinations of scaling can be considered and these are shown in Table 3.0.1. Schematic flow configurations are also given in Figure 3.0.1.

Case I presents a problem which is exactly the same as that of fully wetted propeller flows but with a difference existing in the flow configuration of the inner solution. Instead of using a fully wetted single foil flow, a supercavitating flow must be employed for the inner solution. In this case, the ratios of c to ℓ_c and d to R are assumed to be all of the same order so that, as the propeller blade collapses to a line, all pertinent informa-

tion for the propeller flow can be expressed around the lifting line.

However, this is not the case for Case II in Table 3.0.1. Since we have a long cavity behind each blade, even with the blade shrinking to a lifting line, the cavity portion fails to collapse to a line but remains as a finite length in the outer flow. This portion cannot possibly be represented by any quantities on the lifting line but requires the concept of source sheet.

It will be readily understood that the strength of these source distributions cannot be matched through the expansion of the inner and outer solutions around the lifting line. The reason is that the source strengths of such cavity sheet have nothing to do with the scaling of $c/R = O(\epsilon)$ but belong to the other scaling, i.e., λ_c/R . It is considered that the determination of the source sheet characteristics requires a different type of matching with the inner solution as will be seen later.

The type of problems associated with Cases III and IV are more complex. As the chord shrinks to a line for the outer solution, the spacings between the blades will become unrecognizable since the spacing-to-radius ratio is assumed to be of the same order as that of the chord-to-radius ratio. The outer solution will have to be solved with the actuator disk concept. If the line source term S_0 is equal to zero and no source sheet exists (most likely in Case III), only a careful consideration for choice of the inner flow configuration may be necessary. However, if S_0 is not zero followed by a source sheet, the actuator disk will have to add a source disk as well as the lower pressure region behind it. This will account for the flow retardation effect in the heavily cavitating propeller flow, first explained by Tulin (1965).

In the present work, due to the limited time available, only the first two cases will be solved with the singular perturba-

tion method, leaving the other two cases to the near future effort when resources become available.

3.1 SHORT CAVITY PROPELLER CASE (CASE 1)

3.1.1 Outer Solution

An outer solution, valid in the outer region, will be obtained as a limiting form of ϕ when the blade shrinks to a lifting line. First look at ϕ_V in Equation (2.1.6). By defining the third integral in (2.1.6),

$$I(r', \theta') \equiv \int_{-\infty}^{x-\theta' \lambda} \frac{N_V}{R_V^3} dv, \quad (3.1.1)$$

we can expand $I(r', \theta')$ for small θ' , i.e.,

$$I(r', \theta') = I(r', 0) + \frac{\partial I}{\partial \theta'} \Big|_{\theta'=0} \theta' + \text{H.O.T.} \quad (3.1.2)$$

where H.O.T. stands for the neglected higher-order terms, $O(\theta'^2)$, etc., and

$$I(r', 0) = \int_{-\infty}^x \frac{N_V}{R_V^3} dv \quad (3.1.3)$$

$$\frac{\partial I}{\partial \theta'} \Big|_{\theta'=0} = \frac{\partial}{\partial \theta'} \int_{-\infty}^{x-\theta' \lambda} \frac{N_V}{R_V^3} dv = -\lambda \frac{r' x + r \lambda \sin \psi_k}{R_0^3} \quad (3.1.4)$$

$$R_0 = \left[x^2 + r'^2 + r^2 - 2rr' \cos(-\theta + \sigma_k) \right]^{1/2} \quad (3.1.5)$$

$$\psi_k = -\theta + \sigma_k.$$

We now have ϕ_V in expansion

$$\phi_V = -\frac{1}{2} \sum_{k=1}^K \int_{r_h}^1 \int_{\theta_L}^{\theta_T} \Delta \hat{p}(r', \theta') \left[\int_{-\infty}^x \frac{N_V}{R_V^3} dv - \lambda \theta' \frac{r' x + r \lambda \sin \psi_k}{R_0^3} + \text{H.O.T.} \right] dr' d\theta'. \quad (3.1.6)$$

Redefining some of the terms in this integral, i.e.,

$$\hat{\Delta p}(r, \theta) = \gamma_c(r, \theta) \frac{(r^2 + \lambda^2)^{\frac{1}{2}}}{\lambda}$$

$$\Gamma(r') \equiv \int_{\theta_L}^{\theta_T} \gamma_c(r', \theta') d\theta'$$

$$u_{1x}(r') \equiv \int_{\theta_L}^{\theta_T} \lambda \theta' \hat{\Delta p}(r', \theta') r' d\theta'$$

$$u_{1y}(r') = \int_{\theta_L}^{\theta_T} \lambda^2 \theta' \hat{\Delta p}(r', \theta') d\theta',$$

where the normalization factor for $\Gamma(r)$, i.e., $2\pi RU$, has been used and γ_c denotes the vortex distribution.

Equation (3.1.6) can be written as follows

$$\begin{aligned} \phi_V = -\frac{1}{2} \sum_{k=1}^1 & \left\{ \int_{r_h}^1 \Gamma(r') dr' \left[\int_{-\infty}^x \frac{N_V}{R_V^3} dv \right] \right. \\ & \left. - \int_{r_h}^1 \frac{x u_{1x}(r') + r \sin(-\theta + \sigma_k) \cdot u_{1y}(r')}{R_0^3} dr' + H.O.T. \right\} \quad (3.1.7) \end{aligned}$$

It is seen from Equation (3.1.7) that the potential ϕ_V is composed of a line circulation as the lowest term, moment terms having the axes in the direction of chord and that normal to the blade, and H.O.T.

Similarly, the potential ϕ_s in Equation (2.1.8) will be expanded for small θ' with the present assumption of short cavity in mind. As $\theta' \rightarrow 0$,

$$\frac{1}{R_{\theta'}} = \frac{1}{R_0} + \frac{\partial}{\partial \theta'} \left(\frac{1}{R_{\theta'}} \right)_{\theta'=0} \theta' + \text{H.O.T.} , \quad (3.1.8)$$

and

$$\frac{\partial}{\partial \theta'} \left(\frac{1}{R_{\theta'}} \right)_{\theta'=0} = \frac{\lambda x - rr' \sin \psi_k}{R_0^3} , \quad (3.1.9)$$

therefore,

$$\begin{aligned} \phi_s &= -\frac{1}{2} \sum_{k=1}^k \left[\int_{r_h}^1 \frac{dr'}{R_0} \int_{\theta_L}^{\theta_E} s(r', \theta') d\theta' \right. \\ &\quad \left. + \int_{r_h}^1 \frac{dr'}{R_0^{3/2}} \int_{\theta_L}^{\theta_E} s(r', \theta') \cdot \theta' \cdot (-\lambda r' x + r \lambda \sin \psi_k) d\theta' + \text{H.O.T.} \right] \end{aligned} \quad (3.1.10)$$

With a new definition for the following integrals

$$s_0(r') = \int_{\theta_L}^{\theta_E} s(r', \theta') d\theta' ,$$

$$s_{1x}(r') = \int_{\theta_L}^{\theta_E} s(r', \theta') \theta' (-\lambda r') d\theta' ,$$

$$s_{1y}(r') = \int_{\theta_L}^{\theta_E} s(r', \theta') \theta' d\theta' ,$$

Equation (3.1.10) will be written as

$$\varphi_s = -\frac{1}{2} \sum_{k=1}^K \left[\int_{r_h}^1 \frac{s_0(r')}{R_0} dr' + \int_{r_h}^1 \frac{x s_{1x}(r') + r \sin \psi_k \cdot s_{1y}(r')}{R_0^{3/2}} dr' + \text{H.O.T.} \right]. \quad (3.1.11)$$

In this equation s_0 , s_{1x} and s_{1y} can be interpreted as a line source, the first moment of source in the direction of x and y , respectively.

For matching purposes, the asymptotic limit of the outer solution φ as $s_0 \rightarrow 0$ is required where $s_0^2 = x^2 + y^2$. The first term in Equation (3.1.7) represents the potential, denoted by $\varphi_{V\Gamma}$, due to the vortex line and its free vortices. It is rather difficult to expand this term directly and thus the velocity components, $u_{a\Gamma}$ and $u_{t\Gamma}$, will be used for this purpose, i.e.,

$$u_{a\Gamma} \equiv \frac{\partial \varphi_{V\Gamma}}{\partial x}, \quad u_{t\Gamma} \equiv \frac{\partial \varphi_{V\Gamma}}{\partial y} \quad (3.1.12)$$

where

$$\varphi_{V\Gamma} = -\frac{1}{2} \sum_{k=1}^K \int_{r_h}^1 \Gamma(r') dr' \int_{-\infty}^x \frac{N_k}{R_k^3} dv. \quad (3.1.13)$$

Taking derivatives of $\varphi_{V\Gamma}$ with respect to x and y , we find

$$u_{a\Gamma} = u_{a\Gamma B} + u_{a\Gamma F} \quad (3.1.14)$$

$$u_{t\Gamma} = u_{t\Gamma B} + u_{t\Gamma F} \quad (3.1.15)$$

where

$$u_{a\Gamma B} = -\frac{1}{2} \sum_{k=1}^K \int_{r_h}^1 \Gamma(r') dr' \frac{r \sin \psi_k}{R_0^3} \quad (3.1.16)$$

$$u_a \equiv u_{a\Gamma F} = -\frac{1}{2} \sum_{k=1}^K \int_{r_h}^1 \Gamma(r') dr' \left[\frac{\partial}{\partial r'} \int_{-\theta}^{\infty} \frac{r'(r' - r \cos \psi_\tau)}{R_\tau^3} d\tau \right] \quad (3.1.17)$$

$$u_{t\Gamma B} = \frac{1}{2} \sum_{k=1}^K \int_{r_h}^1 \Gamma(r') dr' \frac{-x \cos \psi_k}{R_0^3} \quad (3.1.18)$$

$$u_t \equiv u_{t\Gamma F} = \frac{1}{2} \sum_{k=1}^K \int_{r_h}^1 \Gamma(r') dr' \cdot$$

$$\cdot \left[\frac{\partial}{\partial r'} \int_{-\theta}^{\infty} \frac{\lambda(r - r' \cos \psi_\tau) + \{x - \lambda(\tau + \theta)\} r' \sin \psi_\tau}{R_\tau^3} d\tau \right] \quad (3.1.19)$$

$$\left. \begin{aligned} \psi_k &= -\theta + \sigma_k \\ \psi_\tau &= \tau + \sigma_k \\ R_\tau &= \left[(\lambda \tau)^2 - 2rr' \cos \psi_\tau + r^2 + r'^2 \right]^{1/2} \end{aligned} \right\} \quad (3.1.20)$$

and the subscripts B and F for the velocity components denote "Bound" and "Free" vortices, respectively.

The dominating term in $u_{a\Gamma B}$ of Equation (3.1.16) comes from $k=1$, the vortex line of its own, as $s_0^2 = x^2 + y^2 \rightarrow 0$, therefore

$$u_{a\Gamma B} \sim \frac{r \sin \theta}{2} \int_{r_h}^1 \frac{\Gamma(r') dr'}{R_{00}^3} + \text{H.O.T.} \quad (3.1.21)$$

where

$$R_{00} = \left[s_0^2 + (r - r')^2 \right]$$

$$s_0^2 = x^2 + y^2$$

$$y = r \sin \theta.$$

The integral in Equation (3.1.21) is singular as $s_0 \rightarrow 0$ and cannot be expanded easily as it is. One of the techniques, among others, to resolve this type of situation is an application of the Fourier integral representation for $1/R_{00}^3$, the method having been used by Ogilvie (1972) and James (1975) in similar problems, i.e.,

$$\begin{aligned} \frac{1}{R_{00}^3} &= -\frac{1}{s_0} \frac{\partial}{\partial s_0} \left(\frac{1}{R_{00}} \right) = \left(s_0^2 + a^2 \right)^{-\frac{3}{2}} = \\ &= -\frac{1}{s_0} \frac{\partial}{\partial s_0} \left[\frac{1}{\pi} \int_{-\infty}^{\infty} K_0(|m|s_0) \exp(-ima) dm \right] \end{aligned} \quad (3.1.22)$$

where K_0 is the modified Bessel function and

$$a = |\mathbf{r} - \mathbf{r}'|. \quad (3.1.23)$$

The expansion of $K_0(|m|s_0)$ can be made as $s_0 \rightarrow 0$ (see Handbook of Mathematical Functions by Abramowitz (1964)),

$$K_0(|m|s_0) \sim -\ln s_0 + O(s_0^2 \ln s_0). \quad (3.1.24)$$

Substitution of (3.1.24) into (3.1.21) and (3.1.22) yields

$$\begin{aligned} u_{AB} &\sim \frac{r \sin \theta}{2} \int_{r_h}^1 \Gamma(r') dr' \left[\frac{1}{\pi} \int_{-\infty}^{\infty} -\frac{1}{s_0} \frac{\partial}{\partial s_0} (-\ln s_0 + H.O.T.) \right. \\ &\quad \left. \cdot \exp(-ima) dm \right] \\ &\sim \frac{r \sin \theta}{2 \pi s_0^2} \int_{r_h}^1 \Gamma(r') dr' \int_{-\infty}^{\infty} \exp(-ima) dm + H.O.T. \\ &\sim \frac{r \sin \theta}{2 \pi s_0^2} \int_{-\infty}^{\infty} dm \left[\int_{r_h}^r \Gamma(r') \exp\{-im(r-r')\} \cdot dr' \right] \end{aligned}$$

$$+ \int_r^1 \Gamma(r') \exp\{-im(r'-r)\} \cdot dr' \Big] + H.O.T. \quad (3.1.25)$$

Integration by parts is applied to Equation (3.1.25),

$$u_{a\Gamma B} \sim \frac{r \sin \theta}{2\pi s_0^2} \int_{-\infty}^{\infty} dm \left[\frac{2\Gamma(r)}{im} - \int_{r_h}^r \frac{d\Gamma(r')}{dr'} \frac{\exp\{-im(r-r')\}}{im} dr' \right. \\ \left. - \int_r^1 \frac{d\Gamma(r')}{dr'} \frac{\exp\{-im(r'-r)\}}{-im} dr' \right] + H.O.T. \quad (3.1.26)$$

Now the method of contour integral will be used by defining

$$I_1 = \int_C \frac{\exp(-ip_1 z)}{iz} dA = 0 \quad (3.1.27)$$

where the contour C to be taken is shown in Figure 3.1.1 and $p_1 = r - r' > 0$. Thus,

$$\int_{-\infty}^{\infty} \frac{\exp(-ip_1 m)}{im} dm + \pi + \int_0^{-\pi} \frac{\exp(-ip_1 (R \cos \theta + Ri \sin \theta))}{iRe^{i\theta}} iRe^{i\theta} d\theta = 0.$$

Since the last integral is zero as $R \rightarrow \infty$,

$$\int_{-\infty}^{\infty} \frac{\exp(-ip_1 m)}{im} dm = -\pi, \quad p_1 = r - r' > 0 \quad (3.1.28)$$

Similarly

$$\int_{-\infty}^{\infty} \frac{\exp(-ip_2 m)}{-im} dm = +\pi, \quad p_2 = r' - r > 0. \quad (3.1.29)$$

$u_{a\Gamma B}$ in Equation (3.1.14) becomes

$$\begin{aligned}
 u_{a\Gamma B} &\sim \frac{r \sin \theta}{a \pi s_0^2} \left[- \int_{r_h}^r \frac{d\Gamma(r')}{dr'} (-\pi) dr' - \int_r^1 \frac{d\Gamma(r')}{dr'} \pi dr' \right] + \text{H.O.T.} \\
 &\sim \Gamma(r) \left[\frac{r \sin \theta}{s_0^2} + \text{H.O.T.} \right] \\
 &\sim \Gamma(r) \left[\frac{y}{x^2 + y^2} + \text{H.O.T.} \right]
 \end{aligned} \tag{3.1.30}$$

where $\Gamma(1) = \Gamma(r_h) = 0$ and $\int_{-\infty}^{\infty} \frac{\Gamma(r)}{im} dm = 0$ have been used.

In the similar manner, $u_{t\Gamma B}$ in Equation (3.1.18) can be expanded

$$u_{t\Gamma B} \sim \Gamma(r) \left[\frac{-x}{x^2 + y^2} + \text{H.O.T.} \right] \tag{3.1.31}$$

It is well known that the induced velocities due to the free vortex sheets, u_a and u_t in Equations (3.1.17) and (3.1.18), have finite values as $x^2 + y^2 \rightarrow 0$, i.e., on the lifting line itself. The final forms of the expansions for u_a and u_t are therefore written

$$u_{a\Gamma} \sim \Gamma(r) \frac{y}{x^2 + y^2} + u_a + \text{H.O.T.} \tag{3.1.32}$$

$$u_{t\Gamma} \sim \Gamma(r) \frac{-x}{x^2 + y^2} + u_t + \text{H.O.T.} \tag{3.1.33}$$

By using the following relationship

$$\Gamma \tan^{-1} \frac{y}{x} = \frac{y}{x^2 + y^2} \mathbf{i} + \frac{-x}{x^2 + y^2} \mathbf{j}, \tag{3.1.34}$$

\hat{v}_Γ becomes

$$\begin{aligned}
 \hat{v}_\Gamma &\sim \Gamma(r) \tan^{-1} \frac{y}{x} + (u_a \cdot \mathbf{x} + u_t \cdot \mathbf{y}) + \text{H.O.T.}, \\
 &\quad \text{as } x^2 + y^2 \rightarrow 0.
 \end{aligned} \tag{3.1.35}$$

The moment term of ϕ_V in Equation (3.1.7), i.e., ϕ_{VM} , can also be expanded by using the method of Ogilvie (1970)

$$\begin{aligned}\phi_{VM} &\equiv \int_{r_h}^1 \frac{xu_{1x}(r') + r \sin(-\theta)u_{1y}(r')}{R_0^3} dr' \\ &\sim \frac{u_{1x}(r) \cdot x + u_{1y}(r) \cdot y}{x^2 + y^2} + \text{H.O.T.} \quad (3.1.36)\end{aligned}$$

where only $k = 1$ has been used for the leading term of ϕ_{VM} .

For the potential due to the source, again the method of the Fourier representation for $1/R_0$ and that of Ogilvie are used for the expansion, which provides

$$\phi_S \sim S_0(r) \ln(x^2 + y^2)^{\frac{1}{2}} - \frac{s_{1x}(r) \cdot x + s_{1y}(r) \cdot y}{x^2 + y^2} + \text{H.O.T.} \quad (3.1.37)$$

Combining ϕ_{VR} , ϕ_{VM} and ϕ_S in Equations (3.1.35, 36 and 37), the two-term expansions of the outer solution ϕ can finally be written as

$$\begin{aligned}\phi &\sim \phi_0 + \Gamma(r) \tan^{-1} \frac{y}{x} + S_0(r) \ln(x^2 + y^2)^{\frac{1}{2}} + (u_a(r) \cdot x + u_t(r) \cdot y) \\ &\quad + \frac{u_{1x}(r) \cdot x + u_{1y}(r) \cdot y}{x^2 + y^2} - \frac{s_{1x}(r) \cdot x + s_{1y}(r) \cdot y}{x^2 + y^2} + \text{H.O.T.} \quad (3.1.38)\end{aligned}$$

where ϕ_0 is the uniform flow part

$$\phi_0 = Ux - rw y. \quad (3.1.39)$$

3.1.2 Inner Solution

The inner solution will be obtained by stretching the coordinates with a suitable stretching factor, in this case the reverse of the blade aspect ratio ε . The three-dimensional Laplace equation becomes the two-dimensional one with an accuracy to the second order of ε . The boundary conditions near and on the

blade remain the same whereas those at infinity points lose their meanings due to the stretching of the coordinates. Since much literature has already described the detailed procedure in similar problems, the formal coordinate expansions, etc., will be deleted herein.

Figure 3.1.2 shows a flow configuration for the inner solution on the new coordinate system attached to the blade. The relationship between the old and new coordinate systems is given as follows

$$\left. \begin{aligned} x &= \bar{x} \sin \beta(r) - \bar{y} \cos \beta(r) \\ y &= -\bar{x} \cos \beta(r) - y \sin \beta(r). \end{aligned} \right\} \quad (3.1.40)$$

or

$$\gamma = -i \bar{\gamma}^* e^{i\beta}$$

where

$$\gamma = x + iy, \bar{\gamma} = \bar{x} + i\bar{y}, \bar{\gamma}^* = \bar{x} - i\bar{y}. \quad (3.1.41)$$

The selection of a cavity closure model to be used for the present singular perturbation problem needs particular attention. In this problem the assumption was made that the cavity length be short and can collapse to a line in the coordinate stretching procedure. This assumption immediately eliminates the chance of using a cavity closure model in which the information in the inner region carried over to the outer region. The open wake model and double spiral vortex model are included in such category. The only feasible one is the single spiral vortex model of Tulin (1964). In this model the physical quantities on the upper and lower wakes are assumed to be identical for the same velocity potential value so that the body-cavity streamlines are closed at the cavity end point in the complex potential plane.

The nonlinear solution method for supercavitating flows with the single spiral vortex model has already been described in Section 2.2.

In order to be able to match the inner solution with the outer solution, the former must be expanded in terms of the velocity potential ϕ . From Equation (2.2.3),

$$d\bar{\gamma} = \frac{dW}{q_\sigma} e^{i\omega} = \frac{e^{i\omega}}{q_\sigma} \frac{dW}{d\zeta} \cdot d\zeta \quad (3.1.42)$$

but $dW/d\zeta$ can be calculated from Equation (2.2.2), thus

$$d\bar{\gamma} = \frac{e^{i\omega}}{q_\sigma} a^2 \frac{2\zeta}{(\zeta^2 + a^2)^2} d\zeta. \quad (3.1.43)$$

Expansion will be carried out as $|\bar{\gamma}| \rightarrow \infty$ or $\zeta \rightarrow ia$ in the ζ -plane, therefore.

$$\begin{aligned} e^{i\omega(\zeta)} &= e^{i\{\omega(ia) + \omega'(ia)(\zeta - ia) + \omega''(ia) \frac{(\zeta - ia)^2}{2} + \dots\}} \\ &= e^{i\omega(ia)} \{1 + K_1 \cdot (\zeta - ia) + K_2 \cdot (\zeta - ia)^2 + \dots\} \quad (3.1.44) \end{aligned}$$

where

$$\left. \begin{aligned} K_1 &= i \omega'(ia) \\ K_2 &= \left[i \omega'(ia) - \{\omega'(ia)\}^2 \right] / 2. \end{aligned} \right\} \quad (3.1.45)$$

$$\omega(ia) = \alpha_I + i \ln \frac{q_I}{q_\sigma}$$

α_I , q_I = incoming flow angle and velocity, respectively, at upstream infinity in the inner flow region.

It must be mentioned that α_I and q_I are quantities yet to be known and thus should not be interpreted as those of the outer flow region at this stage of the theory. They will shortly be determined through the matching procedure. $d\bar{\gamma}$ in Equation (3.1.43) now becomes

$$q_I e^{-i\alpha_I} d\bar{\gamma} \sim -\frac{ia\zeta}{2} \left[\frac{1}{(\zeta - ia)^2} + \frac{K_1}{\zeta - ia} + K_2 + O(\zeta - ia) \right] d\zeta$$

as $\zeta \rightarrow ia$,

by integration

$$q_I e^{-i\alpha_I \frac{1}{\gamma}} \sim -\frac{i\alpha_I}{2} \left[-\frac{1}{\zeta - ia} + K_1 \ln(\zeta - ia) + K_0 + K_2 (\zeta - ia) \right. \\ \left. + O\left((\zeta - ia)^2\right) \right] \quad (3.1.46)$$

where K_0 is an integration constant.

Inversion of Equation (3.1.46) yields to

$$\frac{1}{\zeta - ia} \sim A_0 \bar{\gamma} - K_1 \ln \bar{\gamma} + (-K_1 \ln A_0 + K_0) + K_1^2 \frac{\ln \bar{\gamma}}{A_0 \bar{\gamma}} + \frac{-K_1 L_0 + K_2}{A_0 \bar{\gamma}} \\ + O\left(\frac{\ln \bar{\gamma}}{\bar{\gamma}^2}\right),$$

$$\text{where } A_0 = q_I e^{-i\alpha_I} / i\alpha_I / 2$$

$$L_0 = -K_1 \ln A_0 - K_0$$

which is substituted into W in Equation (2.2.2), providing

$$W \sim q_I e^{-i\alpha_I \frac{1}{\gamma}} + \frac{i\alpha_I}{2} \omega'(ia) \ln \bar{\gamma} + \frac{i\alpha_I}{2} \left\{ -i \omega'(ia) \ln A_0 + K_0 \right\} \\ + \{\omega'(ia)\}^2 \frac{i\alpha_I}{2} \frac{1}{q_I e^{-i\alpha_I}} \frac{\ln \bar{\gamma}}{\bar{\gamma}} + \frac{a^2 \alpha_I^2}{4} \frac{K_1 L_0 - K_2}{q_I e^{-i\alpha_I}} \frac{1}{\bar{\gamma}} \\ + O\left(\frac{\ln \bar{\gamma}}{\bar{\gamma}^2}\right), \text{ as } \bar{\gamma} \rightarrow \infty \quad (3.1.47)$$

Take the complex conjugate on both sides of Equation (3.1.47) and express the quantities of complex conjugate by $*$,

$$W^* \sim q_I e^{i\alpha_I \frac{1}{\gamma^*}} + \frac{i\alpha_I}{2} \omega'(ia)^* + M_0^* + M_1^* \frac{\ln \bar{\gamma}^*}{\bar{\gamma}^*} \\ + M_2^* \frac{1}{\bar{\gamma}^*} + O\left(\frac{\ln \bar{\gamma}^*}{\bar{\gamma}^*}\right). \quad (3.1.48)$$

$$\text{where } M_0^* = \frac{i\alpha_I}{2} \left\{ -i \omega'(ia) \ln A_0 - K_0 \right\}$$

$$M_1 = \left\{ \omega' (ia) \right\}^2 \frac{i a \omega}{2} . \quad (3.1.49)$$

$$M_2 = \frac{a^2 \omega}{4} \frac{K_1 L_0 - K_2}{q_I e^{-iaI}} .$$

Substitution of Equation (3.1.41) into (3.1.48) will provide

$$W^* \sim q_I e^{i(\alpha_I - \beta + \frac{\pi}{2})} \cdot \gamma + \frac{a \omega}{2} \omega' (ia) * \ln \gamma \\ + M_0' + M_1' \cdot \frac{\ln \gamma}{\gamma} + M_2' \cdot \frac{1}{\gamma} + O\left(\frac{\ln \gamma}{\gamma}\right) \quad (3.1.50)$$

where

$$\left. \begin{aligned} M_0' &= M_0^* + \frac{a \omega}{2} \omega' (ia) * \ln i e^{-i\beta} \\ M_1' &= M_1^* \frac{1}{i e^{-i\beta}} \\ M_2' &= \frac{M_2^* + M_1^* \ln i e^{-i\beta}}{i e^{-i\beta}} \end{aligned} \right\} \quad (3.1.51)$$

and W^* is the complex conjugate of W , i.e., $W^* = \phi - i\psi$. The real part of W^* represents the velocity potential ϕ , then

$$\phi \sim q_I \left\{ \cos(\alpha_I - \beta + \frac{\pi}{2}) \cdot x - \sin(\alpha_I - \beta + \frac{\pi}{2}) \cdot y \right\} \\ + \frac{a \omega}{2} \left\{ I_m[\omega' (ia)] \cdot \tan^{-1} \frac{y}{x} + R_e[\omega' (ia)] \ln \left(x^2 + y^2 \right)^{\frac{1}{2}} \right\} \\ + R_e[M_0'] + R_e[M_1' \frac{(x - iy) \ln(x + iy)}{x^2 + y^2}] \\ + \frac{R_e[M_2'] \cdot x + I_m[M_2'] \cdot y}{x^2 + y^2} + O\left(\frac{\ln \gamma}{\gamma}\right), \text{ as } \gamma = x + iy \rightarrow \infty, \quad (3.1.52)$$

where $R_e[M_2']$ and $I_m[M_2']$ denote the real and imaginary parts of M_2' , respectively.

3.1.3 Matching Procedure

The matching procedure for the singular perturbation method is also explained in much literature. This includes the works by Van Dyke (1964), Ogilvie (1970), Brockett (1972) and James (1975). It is stated in the book by Van Dyke (1964) that the asymptotic matching principle will be satisfied by "matching the m -term inner expansion of the n -term outer expansion with the n -term outer expansion of the m -term inner expansion" where m and n are any two integers. Due to the ample literature existing on the subject, the matching steps herein will be followed without formal procedure. It was for the reason that the inner and outer expansions of the outer and inner solutions in the previous sections were made without expanding the coordinate variables. However, in using such an informal approach, care must be taken for the order of magnitude of each term in matching. The matching will be carried out for the velocity potentials ϕ in Equations (3.1.38) and (3.1.52).

The zeroth order matching will determine the unknown velocity amplitude and direction, q_I and α_I of the inner flow field as follows:

$$q_I^{(1)}(r) = \left\{ U^2 + (r\omega)^2 \right\}^{\frac{1}{2}} + O(\varepsilon) \quad (3.1.53)$$

and

$$\tan(\alpha_I^{(1)} - \beta + \frac{\pi}{2}) = \frac{r\omega}{U} = \tan^{-1}\left(\frac{\pi}{2} - \beta\right)$$

or

$$\alpha_I^{(1)}(r) = 0 + O(\varepsilon) \quad (3.1.54)$$

where

$$O(\varepsilon) < O(1) \text{ and}$$

$$\varepsilon = \frac{1}{AR}$$

$$AR = \frac{\text{Propeller Blade Area}}{\text{Propeller Radius}}.$$

It should be mentioned that the inner flow region has been selected to have the coordinate system, (\bar{x}, \bar{y}) in line with the hydrodynamic flow direction made with U and u_r (see Figure 3.1.2). The superscripts on q_I and α_I denote the quantities of first order matching.

The first order matching will further be carried out for determining the strength of circulation Γ . As a result of the zeroth order matching, the inner cavity flow problem can be solved for the first time. The boundary conditions available for the inner problem include the following:

i) At upstream infinity, i.e., at $\zeta = ia$,

$$\omega(ia) = \alpha_I^{(1)} + i \ln \frac{q_I^{(1)}}{q_\sigma} \quad (3.1.55)$$

where $\omega(\zeta)$, α_I , and q_I are given in Equations (2.2.4), (3.1.53) and (3.1.54), respectively and

$$q_\sigma = q_I^{(1)} \sqrt{1 + \sigma} ,$$

$$\sigma = \frac{p_1 - p_\sigma}{\frac{1}{2} \rho \{q_I^{(1)}\}^2} .$$

ii) The closure condition (see p. 173 of the paper by Larock and Street (1965)) is given by

$$R_e \left\{ \oint_C \omega(\zeta) dW \right\} = 0 ,$$

where C denotes the contour enclosing the body-cavity system, which is transformed into ζ -plane,

$$R_e \left\{ \oint_C \omega(\zeta) \frac{dW}{d\zeta} d\zeta \right\} = 0 , \quad (3.1.56)$$

with the residue theorem employed, finally

$$R_e \left\{ \omega' (ia) \right\} = 0. \quad (3.1.57)$$

where ω' denotes the derivative of ω with respect to ζ . More detailed derivation of Equation (3.1.55) from Equation (3.1.54) is discussed in the paper by Furuya and Maekawa (1980).

iii) The scaling condition between the physical and transform plane states that the wetted portion of the body calculated from the theory should be equal to S specified in the physical plane. On the wetted part of the streamline

$$\frac{d\bar{y}}{ds} = e^{i\bar{\beta}},$$

or

$$ds = e^{-i\bar{\beta}} \frac{e^{i\omega}}{q_\zeta} \frac{dw}{d\xi} d\xi. \quad (3.1.58)$$

where $\bar{\beta} = \tan^{-1}(dy/dx)$ and \bar{y} denotes the body coordinate.

For $-1 < \xi < b$, $\omega(\xi)$ can be written as follows:

$$\omega(\xi) = \begin{cases} i g(\xi) + \bar{\beta}(\xi) , & -1 < \xi < 0 \\ i g(\xi) + \bar{\beta}(\xi) + \pi , & 0 < \xi < b \end{cases}$$

where

$$g(\xi) = \sqrt{(1 + \xi)(b^{(1)} - \xi)} \left\{ -\frac{1}{\pi} \int_{-1}^{b^{(1)}} \frac{\beta(\xi')}{\sqrt{(1 + \xi')}(b^{(1)} - \xi')} \frac{d\xi'}{\xi' - \xi} \right. \\ \left. - \int_0^{b^{(1)}} \frac{1}{\sqrt{(1 + \xi')}(b^{(1)} - \xi')} \frac{d\xi'}{\xi' - \xi} + P^{(1)} \right\},$$

where \oint indicates a Cauchy principle integral and superscript 1 denotes the first order quantities. By integrating Equation (3.1.58) we obtain

$$s(\xi) = \int_{\xi}^{b^{(1)}} sg(\xi) \frac{e^{-g(\xi)}}{\sqrt{1+\sigma}} \frac{dw}{d\xi} d\xi$$

where

$$sg(\xi) = \begin{cases} 1 & \xi > 0 \\ -1 & \xi < 0. \end{cases}$$

The arc length condition is therefore satisfied by the following equation:

$$s - s(-1) = 0. \quad (3.1.59)$$

The four unknown parameters in the inner flow, i.e., $a^{(1)}$, $b^{(1)}$, $P^{(1)}$ and $\phi_\lambda^{(1)}$ will now be uniquely determined by using the above four boundary conditions. It is, of course, understood that these four equations are highly retarded, thus requiring a numerical method such as that introduced by Furuya (1975) for a similar problem.

Once the inner problem is solved above, the first order matching for Γ is readily achieved by comparing the corresponding terms in ϕ for the inner and outer expansion of Equations (3.1.38) and (3.1.52), i.e.,

$$\Gamma^{(1)}(r) = \frac{a^{(1)} \phi_\lambda^{(1)}}{2} - I_m [\omega'(ia^{(1)})] + O(\epsilon^2). \quad (3.1.60)$$

It must be mentioned that the right-hand side of Equation (3.1.60) is the totally known quantity obtained by solving the inner solution. It is also important to notice for the latter matching procedure that $\Gamma^{(1)}(r)$, therefore $a\phi_\lambda/2$, $I_m [\omega'(ia)]$ are quantities of order ϵ .

The source term $S_0(r)$ in the inner expansion of the outer solution is matched with the corresponding term in the counterpart, but it should be zero due to the closure condition applied to the inner solution (i.e., Equation (3.1.57)),

$$S_0^{(1)}(r) = \frac{a^{(1)} \rho \lambda^{(1)}}{2} R_e [\omega' (ia^{(1)})] \equiv 0. \quad (3.1.61)$$

In order to carry out the second order matching, the second order inner solution must be considered. As has been mentioned in the beginning of Section 3.1.2, the two-dimensional Laplace equation still holds with exactly the same boundary conditions and thus the expansion of the inner solution remains the same as that of Equation (3.1.51). The difference in matching, however, exists, particularly in the outer solution; the first order matching has provided the value for $\tau^{(1)}(r)$ in Equation (3.1.38). Once the circulation distribution $\tau^{(1)}(r)$ on the lifting line is known, the induced velocities $u_a^{(1)}(r)$ and $u_t^{(1)}(r)$ in Equation (3.1.38) will be readily calculated from the formula given in Equations (3.1.17) and (3.1.19). Various methods of computing these integrals are available. One of the most popular and convenient methods will be that by Lerb (1952) who applied Nicholson's asymptotic formula for singular integrals. The second order matching will first be made for the incoming flow velocity and direction;

$$q_I^{(2)} = \left[\left\{ U + u_a^{(1)}(r) \right\}^2 + \left\{ r\omega - u_t^{(1)}(r) \right\}^2 \right]^{\frac{1}{2}} + O(\varepsilon^2) \quad (3.1.62)$$

and

$$\tan(\alpha_I^{(2)} - \beta + \frac{\pi}{2}) = \frac{r\omega - u_t^{(1)}(r)}{U + u_a^{(1)}(r)} = \tan\left(\frac{\pi}{2} - \beta + \alpha_i\right)$$

or

$$\alpha_I^{(2)} = \alpha_i + O(\varepsilon^2) \quad (3.1.63)$$

where

$$\alpha_i = \tan^{-1} \left\{ \frac{r\omega - u_t^{(1)}(r)}{u + u_a^{(1)}(r)} \right\} - \left(\frac{\pi}{2} - \beta \right), \quad (3.1.64)$$

and the induced flow angle α_i is depicted in Figure 3.1.2.

The circulation matched to the second order will now be written in the following form,

$$\Gamma^{(2)}(r) = \frac{a^{(2)} \phi_l^{(2)}}{2} I_m [\omega' (ia^{(2)})] + O(\varepsilon^3) \quad (3.1.65)$$

where all quantities of the right-hand side in Equation (3.1.65) must be obtained with a new set of the upstream flow conditions, i.e., $q_I^{(2)}$ and $\alpha_I^{(2)}$ which are defined in Equations (3.1.62) and (3.1.63). The matching for the source term remains the same as before,

$$S_0^{(2)} = \frac{a^{(2)} \phi_l^{(2)}}{2} R_e [\omega' (ia^{(2)})] \equiv 0. \quad (3.1.66)$$

The moment terms in Equation (3.1.38) will be matched with the corresponding terms in Equation (3.1.50);

$$\left. \begin{aligned} u_{1x}(r) - s_{1x}(r) &= R_e [M_2'] + O(\varepsilon^3) \\ u_{1y}(r) - s_{1y}(r) &= I_m [M_2'] + O(\varepsilon^3) \end{aligned} \right\} \quad (3.1.67)$$

The result of this matching indicates that the moment due to the circulation distribution or that due to the source distribution cannot be distinguished within the framework of the singularity distribution method. However, practically more control for the circulation distribution can be possible than that for the source distribution so that the former will be exercised in actual propeller design work.

It can be realized now that the results of the matching procedure take a somewhat different form from that in other conventional methods such as those of Van Dyke (1964), Ogilvie (1970), Brockett (1972) and James (1975). In those works, the circulation Γ was expanded as an ascending series of ε ,

$$\Gamma = \sigma_1(\varepsilon) \Gamma^{(1)} + \sigma_2(\varepsilon) \Gamma^{(2)} + \dots$$

where

$$O(\sigma_n(\varepsilon)) > O(\sigma_{n+1}(\varepsilon)).$$

This type of expansion was not possible in the present approach since the nonlinear theory was applied to the inner solution. Change of the circulation $\Delta\Gamma$ due to that of the upstream flow condition is not additive to $\Gamma^{(1)}$. Therefore, after each matching procedure, Γ should be successively rewritten as follows

$$\Gamma(r) = \Gamma^{(1)}(r) + O(\varepsilon^2) \quad \text{after the first order matching}$$

$$\Gamma(r) = \Gamma^{(2)}(r) + O(\varepsilon^3) \quad \text{after the second order matching}$$

⋮

and so on.

Finally, it should be mentioned that the third term from the last in Equation (3.1.50) was not left out for matching. It is readily seen from Equations (3.1.49) and (3.1.51) that M' is of an order ε so that the whole term has an order of $\varepsilon^2 \ln \varepsilon$. This is a higher order than that of the next term and, as a matter of fact, the same order as that of the last term. Matching for this term cannot be possible within the second order matching but will require the higher order inner and outer solutions.

3.1.4 Propeller Performance

The thrust and torque coefficients of a propeller can be calculated based on the circulation, flow velocity and angle.

The local lifting force ΔL is obtained from the Kutta-Joukowski law

$$\Delta L(r) = \rho \left\{ \left(U + u_a^{(1)}(r) + \dots \right)^2 + \left(r \omega - (u_t^{(1)}(r) + \dots) \right) \right\}^{\frac{1}{2}} \bar{\Gamma}(r). \quad (3.1.68)$$

It should be mentioned that all quantities in this equation are dimensional ones, whereas throughout the analysis in Section 3 the normalized ones were used. This point was mentioned in Section 2 in which the nondimensional $\bar{\Gamma}$ was defined as

$$\bar{u}_a^{(1)}(\bar{r}) = u_a^{(1)}(r)/U$$

$$\bar{u}_t^{(1)}(\bar{r}) = u_t^{(1)}(r)/U$$

$$\bar{\Gamma}(\bar{r}) = \Gamma/2 UR$$

$$\bar{r} = r/R$$

but the bars above the letters had been dropped for convenience.

The thrust force T_h and power P_w of the propeller are thus written

$$T_h = K \int_0^R \Delta L(r) \cos(\beta(r) + \alpha_i) dr$$

$$P_w = K \int_0^R \omega r \Delta L(r) \sin(\beta(r) + \alpha_i) dr.$$

Conventional normalization provides the thrust and power coefficients, C_T and C_p ,

$$\begin{aligned}
 C_T &= \frac{T_h}{\frac{1}{2} \rho U^2 \pi R^2} \\
 &= 4 K \int_0^1 \left\{ \left(1 + u_a^{(1)}(r) + \dots \right)^2 + \left(\frac{r}{\lambda} - (u_t^{(1)}(r) + \dots) \right)^2 \right\} \\
 &\quad \cdot \Gamma(r) \cos(\beta(r) + \alpha_i) dr, \quad (3.1.69)
 \end{aligned}$$

$$\begin{aligned}
 C_p &= \frac{p_n}{\frac{1}{2} \rho U^3 \pi R^2} \\
 &= \frac{4K}{\lambda} \int_0^1 r \cdot \left\{ \left(1 + u_a^{(1)}(r) + \dots \right)^2 + \left(\frac{r}{\lambda} - (u_t^{(1)}(r) + \dots) \right)^2 \right\}^{\frac{1}{2}} \\
 &\quad \sin(\beta(r) + \alpha_i) dr. \quad (3.1.70)
 \end{aligned}$$

3.2 LONG CAVITY PROPELLER CASE (CASE 2)

This is the case in which the cavity length ℓ_c has the same order of magnitude as that of the propeller radius R . As is shown in Table 3.0.1, i.e.,

$$\frac{\ell_c}{R} = O(1)$$

whereas the chord c to the propeller radius ratio remains the same as before,

$$\frac{c}{R} = O(\varepsilon)$$

$$\varepsilon = \frac{1}{AR}$$

$$AR = \frac{\text{Propeller Blade Area}}{\text{Propeller Radius}}.$$

It is interpreted that when the chord shrinks to a lifting line with the propeller radius (or span) fixed, the cavity cannot shrink to a line. The outer solution should therefore consist of a lifting line followed by a cavity sheet as is shown in Figure 3.2.1.(a).

The inner solution obtained with $x = \varepsilon X$, $y = \varepsilon Y$ and $z = Z$ as $\varepsilon \rightarrow 0$ will be the one having the span length and cavity length to be out of sight. Therefore, the formal singular perturbation method would request the inner flow configuration to have an infinite cavity. However, a difficult problem of using such a flow configuration arises in the matching procedure. Since the cavitation number σ may be defined as

$$\sigma = \frac{p_c - p_\infty}{\frac{1}{2} \rho q_\infty^2} \quad (3.2.1)$$

where

p_c , p_∞ = static pressures inside the cavity and at the upstream infinity, respectively,

q_∞ = velocity at the upstream infinity,

the velocity on the cavity wall should be calculated by Bernoulli equation

$$q_c = q_\infty \sqrt{1 + \sigma}.$$

For the infinite cavity problem, the upstream flow velocity in the inner region q_I should be identical to q_c . As a result it is found that

$$q_I = q_c = q_\infty \sqrt{1 + \sigma}. \quad (3.2.2)$$

As has been seen from the previous section, the first order matching will provide

$$q_I = q_\infty \quad (3.2.3)$$

which conflicts the precedent result obtained in Equation (3.2.3). This problem apparently stemmed from the erroneous choice of the inner flow configuration. The rule of the singular perturbation method says that the inner or outer flow solution shall not carry any physical or flow information connecting the counterpart solution. In the above discussion the cavitation number which defines the physical relationship between the cavity of the inner region pressure and the upstream-infinity pressure at the outer region also determined the upstream pressure or velocity q_I of the inner region. This overspecification for the boundary conditions caused a problem of proper matching for determining the unknown quantities.

Because of the reason just mentioned, the inner solution must be obtained by solving a problem for the flow configuration having a finite cavity length. Although the cavity treated in the present case is assumed to be too long to be enclosed

in the inner region, the complete body-cavity system will have to be squeezed within the inner region. A question arises as to what kind of closure condition is to be used. Due to over-stretching the inner coordinate in the present case, one might consider imposing a condition that the total source of the body-cavity system be finite in order to represent the long cavity not to be enclosed in this region. However, there is no way at this stage to determine a quantitative number for the finite total source strength. It is for this reason that the first order inner solution will use $S_o = 0$ and that, if there is any correction, it should come from the matching procedure.

The first-order inner solution in this case is therefore identical to that used in the previous section. The outer expansion of the inner solution in Equation (3.1.52) can be used for the matching purpose.

As far as the inner expansion of the outer solution is concerned, the lifting-line circulation and its free vortex have the same expansion form as Case 1, i.e.,

$$\psi_v(r) \sim \psi(r) \tan^{-1} \frac{y}{x} + (u_a \cdot x + u_t \cdot y) + \frac{\omega_{1x}(r) \cdot x + \omega_{1y}(r) \cdot y}{x^2 + y^2} + \text{H.O.T.} \quad (3.2.4)$$

The difference in the present case, however, exists for the expansion of ψ due to the source terms, ψ_s and its matching with the inner solution. As has been mentioned in the beginning of this section, when $\epsilon \rightarrow 0$ with the span length fixed, the cavity fails to shrink to a line in the present case. The cavity sheet is left over behind the lifting line. Any quantities associated with this cavity sheet cannot be determined by matching on the line because they do not belong to the same stretching factor ϵ . In order to determine $s(r, \theta)$ in Equation (2.1.8), the matching with a new scaling parameter δ will be necessary. The new scaling parameter δ will be defined as the

maximum cavity thickness to the cavity length. In this sense the present problem is categorized as a "multiple" scale problem in the singular perturbation method as is explained in the book by Van Dyke (1964).

The same potential function due to the source singularity as before (Equation (2.1.8)) is used

$$\phi_s(x, r, \theta) = -\frac{1}{2} \sum_{k=1}^K \int_{r_h}^1 \int_{\theta_L}^{\theta_E} \frac{s(r', \theta') dr' d\theta'}{R_{\theta'}}, \quad (3.2.5)$$

$$\begin{aligned} R_{\theta'} &= \left[(x - \lambda \theta')^2 + r'^2 + r^2 - 2r' r \cos \psi_{\theta'} \right]^{\frac{1}{2}} \\ &= \left[(x - \lambda \theta')^2 + (r' - r \cos \psi_{\theta'})^2 + (r \sin \psi_{\theta'})^2 \right]^{\frac{1}{2}}, \end{aligned} \quad (3.2.6)$$

$$\psi_{\theta'} = \theta' - \theta + \sigma_k. \quad (3.2.7)$$

The inner expansion of the outer solution for the new parameter δ will be made as follows. In Equation (3.2.5) $\phi_s(s, r, \theta)$ is expanded as a point of (x, r, θ) approaches the blade-cavity surface in the direction normal to its surface element. By changing the coordinate system from the cylindrical one to a local one (\bar{x}, \bar{y}, r) , attached to the cavity-body surface as is shown in Figure 3.2.2, ϕ_s can be written

$$\phi_{s\delta} \sim -\frac{1}{2} \int_{r-\Delta r}^{r+\Delta r} \int_{\bar{x}-\Delta x}^{\bar{x}+\Delta x} \frac{\bar{s}(r', \bar{x}') dr' d\bar{x}'}{\left[(\bar{x} - \bar{x}')^2 + (r - r')^2 + \bar{y}^2 \right]^{\frac{1}{2}}} + \text{H.O.T.} \quad (3.2.8)$$

where

$$s(r', \theta'(\bar{x}')) = \bar{s}(r', \bar{x}') \sqrt{r'^2 + \bar{y}^2}$$

$$\lambda = U/\omega R,$$

and consideration has been made that the major contribution for $\bar{\phi}_{s\delta}$ arises from the nearest singularity with $\zeta_k = 0$. The subscript δ for ϕ_s has been used to distinguish the expansion in terms of δ from that in ϵ .

In order to expand $\bar{\phi}_{s\delta}$ as $\bar{y} \rightarrow 0$, the Fourier transform method used in Section 3.1.1 will again be employed (see also page 23 of Ogilvie (1970)).

Define an integral $\bar{\phi}_{s\delta}$ as follows

$$\bar{\phi}_{s\delta} = -\frac{1}{2} \int_{-\infty}^{\infty} \int_{-\infty}^{\infty} \frac{\bar{s}(r', \bar{x}) dr' d\bar{x}'}{\left[(\bar{x} - \bar{x}')^2 + (r - r')^2 + \bar{y}^2 \right]^{\frac{1}{2}}} \quad (3.2.9)$$

where

$$\bar{s}(r', \bar{x}) = 0 \quad \text{for } |r' - r| \geq \Delta r$$

$$|\bar{x}' - \bar{x}| \geq \Delta x.$$

The Fourier transform of $\bar{\phi}_{s\delta}$ with respect to \bar{x} , is given by

$$\int_{-\infty}^{\infty} \bar{\phi}_{s\delta} e^{-ik\bar{x}} d\bar{x} = -\frac{1}{2} \int_{-\infty}^{\infty} \int_{-\infty}^{\infty} \int_{-\infty}^{\infty} \frac{\bar{s}(r', \bar{x}') e^{-ik\bar{x}} dr' d\bar{x}' d\bar{x}}{\left[(\bar{x} - \bar{x}')^2 + (r - r')^2 + \bar{y}^2 \right]^{\frac{1}{2}}}.$$

With a change of variables, $t = \bar{x} - \bar{x}'$ and defining the Fourier transform of $\bar{\phi}_{s\delta}$ and \bar{s} by $\bar{\phi}_{s\delta}^*$ and \bar{s}^* , respectively,

$$\begin{aligned} \bar{\phi}_{s\delta}^*(k; r; \bar{y}) &= -\frac{1}{2} \int_{-\infty}^{\infty} \int_{-\infty}^{\infty} \int_{-\infty}^{\infty} \frac{\bar{s}(r', \bar{x}') e^{-ik(t + \bar{x}')} dr' d\bar{x}' dt}{\left[t^2 + (r - r')^2 + \bar{y}^2 \right]^{\frac{1}{2}}} \\ &= -\frac{1}{2} \int_{-\infty}^{\infty} \bar{s}^*(r', k) dr' \int_{-\infty}^{\infty} \frac{e^{-ikt} dt}{\left[t^2 + (r - r')^2 + \bar{y}^2 \right]^{\frac{1}{2}}} \end{aligned}$$

$$= - \int_{-\infty}^{\infty} \bar{s}^*(r', k) dr' \cdot K_0 \left\{ k \left[(r - r')^2 + \bar{y}^2 \right]^{\frac{1}{2}} \right\}$$

where K_0 is the modified Bessel function (see page 9 of Fourier Cosine Transforms Section of the book by Erdélyi (1954)) for the half integral of the real part. The second Fourier transform is taken with respect to r ;

$$\begin{aligned} \bar{s}_{\delta}^{**}(k, m; \bar{y}) &= - \int_{-\infty}^{\infty} \int_{-\infty}^{\infty} \bar{s}^*(r', k) dr' e^{-imr} K_0 \left\{ k \left[(r - r')^2 + \bar{y}^2 \right]^{\frac{1}{2}} \right\} dr' \\ &= - \int_{-\infty}^{\infty} \int_{-\infty}^{\infty} \bar{s}^*(r', k) dr' e^{-im(t + r')} K_0 \left\{ k \left(t^2 + \bar{y}^2 \right)^{\frac{1}{2}} \right\} dt \\ &= - \bar{s}^{**}(k, m) \int_{-\infty}^{\infty} e^{-imt} K_0 \left\{ k \left(t^2 + \bar{y}^2 \right)^{\frac{1}{2}} \right\} dt \\ &= -\pi \frac{\bar{s}^{**}(k, m)}{k^2 + m^2} e^{-|\bar{y}|(k^2 + m^2)^{\frac{1}{2}}} \end{aligned} \quad (3.2.10)$$

where the formula for the Fourier cosine transform of K_0 on page 56 of Erdélyi (1954) has been used and the double stars $**$ for the superscripts denote the double Fourier transform of each function.

Expansion of \bar{s}_{δ}^{**} for small \bar{y} can now be made;

$$\begin{aligned} \bar{s}_{\delta}^{**}(k, m; \bar{y}) &= -\pi \frac{\bar{s}^{**}(k, m)}{(k^2 + m^2)^{\frac{1}{2}}} \left[1 - |\bar{y}|(k^2 + m^2)^{\frac{1}{2}} + \right. \\ &\quad \left. \frac{1}{2} \frac{\bar{y}^2}{(k^2 + m^2)^{\frac{1}{2}}} (k^2 + m^2) + O(\bar{y}^3) \right]. \end{aligned} \quad (3.2.11)$$

Inverting Equation (3.2.11) term by term,

$$\begin{aligned}\phi_{s\delta}(\bar{x}, r, \bar{y}) &= \phi_{s\delta}(\bar{x}, r, 0) + \pi |\bar{y}| \bar{s}(r, \bar{x}) \\ &+ \frac{1}{2} \pi |\bar{y}|^2 \left[\phi_{s\delta}(\bar{x}, r, 0)_{xx} + \phi_{s\delta}(\bar{x}, r, 0)_{zz} \right] + O(\bar{y}^3) \quad (3.2.12)\end{aligned}$$

where $\phi_{s\delta}(x, r, 0)_{xx}$ and $\phi_{s\delta}(x, r, 0)_{zz}$ denote the second derivatives of $\phi_{s\delta}(x, 0, z)$ with respect to x and z , respectively and

$$\phi_{s\delta}(\bar{x}, r, 0) = -\frac{1}{2} \int_{r_h}^1 \int_0^{\lambda_c} \frac{\bar{s}(r', \bar{x}') dr' dx'}{\left[(\bar{x} - \bar{x}')^2 + (r - r')^2 \right]^{\frac{1}{2}}} \quad (3.2.13)$$

There exists a problem in inverting the above equation: the first term in Equation (3.2.12) $\phi_{s\delta}(\bar{x}, r, 0)$ cannot be expressed directly in terms of $\bar{s}(r, \bar{x})$ due to the extra term in Equation (3.2.11), i.e., $(k^2 + m^2)^{\frac{1}{2}}$. In order to determine $\bar{s}(r, \bar{x})$, the second term must be used as will be seen shortly.

The inner solution to be matched with the outer solution expansion in Equation (3.2.13) should be obtained from stretching the coordinates based on the two parameters, ϵ and δ . With $x = \epsilon X$, $y = \epsilon Y$, $z = Z$ and $\delta = \text{maximum cavity thickness}/\lambda_c$ as ϵ and $\delta \rightarrow 0$, the flow configuration will become the one used in a linearized supercavitating flow theory; the body-cavity streamlines are mapped onto a thin slit as is shown in Figure 3.2.1(b). Although it may be possible to expand the nonlinear solution around the \bar{y} -axis, such expansion seems extremely complicated due to the nature of the theory. The purpose of using the linearized theory here is simply to determine the source strength for the cavity thickness. The determination of all other major characteristics still depends on the nonlinear theory. The higher accuracy of the overall results will thus be maintained with the major portion including the circulation to be determined by the nonlinear theory.

As has been described in Section 2.3 for the 2-D linearized supercavitating flow theory, the source distribution on the

body-cavity slit can be obtained as a function of the cavitation number and geometric foil profile. The velocity potential due to the source distribution, expanded in terms of small y , will be expressed in the following form

$$\psi_s \sim v |y| \quad (3.2.14)$$

where

$$v = \begin{cases} \frac{s_1(\bar{x})}{2}, & 0 < \bar{x} < 1 \\ \frac{s_2(\bar{x})}{2}, & 1 < \bar{x} < \lambda_c \end{cases} \quad (3.2.15)$$

and $s_1(\bar{x})$ and $s_2(\bar{x})$ have been given in Equations (2.3.16) and (2.3.17).

Matching between the inner and outer solutions will now determine the unknown source distribution function $\bar{s}(r, \bar{x})$;

$$\bar{s}(r, \bar{x}) = \begin{cases} \frac{s_1(\bar{x})}{2\pi}, & 0 < \bar{x} < 1 \\ \frac{s_2(\bar{x})}{2\pi}, & 1 < \bar{x} < \lambda_c \end{cases}, \quad (3.2.16)$$

$s_1(\bar{x})$ in Equation (2.3.16),

$s_2(\bar{x})$ in Equation (2.3.17).

Once the source distribution is obtained, the outer solution due to the source singularity will be expanded now in terms of ϵ . As the blade chord shrinks to a line, ψ_s is expressed in the similar form to that in Equation (3.1.11),

$$\begin{aligned} \mathbf{\hat{s}}_s = -\frac{1}{2} \sum_{k=1}^K \left[\int_{r_h}^1 \frac{\bar{s}_0(r')}{R_0} dr' + \int_{r_h}^1 \frac{x s_{1x}(r') + r \sin \psi_k \cdot s_{1y}(r')}{R_0} dr', \right. \\ \left. + \int_{r_h}^1 dr' \int_0^{\theta_E} \frac{s_2(r', \theta'(\bar{x}'))}{R_0} d\theta' + \text{H.O.T.} \right] \quad (3.2.17) \end{aligned}$$

where

$$\bar{s}_0(r) = \int_{\theta_L}^{\theta_T} s_1(r', \theta'(\bar{x}')) d\theta' \quad (3.2.18)$$

$$s_{1x}(r') = \int_{\theta_L}^{\theta_T} s_1(r', \theta'(\bar{x}')) \theta'(-\lambda r') d\theta' \quad (3.2.19)$$

$$s_{1y}(r') = \int_{\theta_L}^{\theta_T} s_1(r', \theta'(\bar{x}')) \theta' d\theta' \quad (3.2.20)$$

and s_1 and s_2 are given in Equations (2.3.16) and (2.3.17).

The last term in Equation (3.2.17) is the new term evolving from the existence of the long cavity sheet.

Now the inner expansion of the outer solution as $\varepsilon \rightarrow 0$ becomes

$$\begin{aligned} \mathbf{\hat{s}}_s \varepsilon \sim \bar{s}_0(r) \ln(x^2 + y^2)^{\frac{1}{2}} - \frac{s_{1x}(r) \cdot x + s_{1y}(r) \cdot y}{x^2 + y^2} + \left(u_{as} \cdot + u_{ts} \cdot y \right) \\ + \text{H.O.T.} \quad (3.2.21) \end{aligned}$$

where

$$\left. \begin{aligned} u_{as} &= \frac{\partial \hat{s}_2}{\partial x}, \\ u_{ts} &= \frac{\partial \hat{s}_2}{\partial y} \end{aligned} \right\} \quad (3.2.22)$$

$$\rho_{s2} = -\frac{1}{2} \sum_{k=1}^K \int_{r_h}^1 dr' \int_0^{\theta_E} \frac{s_2(r', \theta'(\bar{x}'))}{R_0} d\theta'. \quad (3.2.23)$$

The two-term inner expansion of the outer solution is now written

$$\begin{aligned} \phi \sim \phi_0 + U(r) \tan^{-1} \frac{y}{x} + \bar{s}_0(r) \ln(x^2 + y^2)^{\frac{1}{2}} + \left\{ (u_a(r) + u_{as}(r)) \cdot x \right. \\ \left. + (u_t(r) + u_{ts}(r)) \cdot y \right\} + \frac{u_{1x}(r) \cdot x + u_{1y} \cdot y}{x^2 + y^2} \\ - \frac{s_{1x}(r) \cdot x + s_{1y}(r) \cdot y}{x^2 + y^2} + \text{H.O.T.} \quad (3.2.24) \end{aligned}$$

where

$$\phi_0 = Ux - r\omega y. \quad (3.2.25)$$

The same matching procedure as in Case I can be applied here. This will result in almost the identical solution as before except for the incoming flow velocity q_I , induced velocities α_i , and the source strength $s_0^{(2)}$;

$$\begin{aligned} q_I^{(2)} = \left[\left\{ U + u_a^{(1)}(r) + u_{as}^{(1)}(r) \right\}^2 + \left\{ r - u_t^{(1)}(r) - u_{ts}^{(1)}(r) \right\}^2 \right]^{\frac{1}{2}} \\ + O(\epsilon^2), \quad (3.2.26) \end{aligned}$$

$$\alpha_I^{(2)} = \alpha_i + O(\epsilon^2), \quad (3.2.27)$$

$$\alpha_i = \tan^{-1} \left\{ \frac{r\omega - u_t^{(1)}(r) - u_{ts}^{(1)}(r)}{U + u_a^{(1)}(r) + u_{as}^{(1)}(r)} \right\} - \left(\frac{\pi}{2} - \beta \right), \quad (3.2.28)$$

$$s_0^{(2)} = \frac{\alpha_I^{(2)} \phi_0^{(2)}}{2} \operatorname{Re} [\omega' (ia^{(2)})] = s_0 \text{ in Equation (3.2.18).} \quad (3.2.29)$$

The result of the second order matching indicates that the second order inner problem to be solved has the incoming flow quantities $q_I^{(2)}$ and $\alpha_I^{(2)}$ with the closure condition $S_0^{(2)} = \bar{S}_0$, finite. It means that (1) the upstream flow now has the induced velocity correction not only due to the vortex wake but also the source sheet and (2) the total source strength is not equal to zero, but finite, given by Equation (3.2.18). The latter condition is interpreted as a correction to the assumption made for the first order inner solution, as has been mentioned earlier. The matching for the circulation of the second order provides exactly the same form as that in Case I, i.e.,

$$\Gamma^{(2)}(r) = \frac{a^{(2)} \alpha_I^{(2)}}{2} I_m [\omega' (ia^{(2)})]. \quad (3.2.30)$$

Table 3.2.1 is provided to help clarify the present matching procedure in comparison with Case I.

4.0

CONCLUSION AND RECOMMENDATION

Unlike finite span wings or subcavitating propellers, the singular perturbation method for the supercavitating propeller required careful classification of the problem due to the existence of the multiple scaling parameters. The scaling parameters here included 1) span length R , 2) chord length c , 3) blade spacing d and 4) cavity length λ_c . The span length R was chosen to be the reference parameter for constructing various scaling parameters, namely c/R , d/R and λ_c/R .

The first problem solved here assumed that c/R and λ_c/R were of order ϵ but d/R was of order of unity. It turned out that the nature of the singular perturbation problem was similar to that for the subcavitating propeller solved by Brockett (1972) except for the solution of the inner region. The thrust and torque coefficients were obtained explicitly without solving the integral equations. Since the nonlinear supercavitating flow theory was employed in the present work as the inner solution, there existed no limitation for the flow incidence angles or blade profile shapes. Due to the nature of the nonlinear theory, the loading coefficients could not be expressed in ascending series of ϵ , but were calculated with new boundary conditions applied. It must be mentioned that the new calculation will not cause any difficulty since the same formula for the boundary value problem can be utilized with changing only the boundary conditions. It is believed that the present solution obtained with the nonlinear theory as the inner solution will provide more accurate results than those with the linearized theory.

The second problem treated in this study was the case in which c/R had an order of ϵ but λ_c/R and d/R were of order of unity. Physically, this was the case having long cavities behind the propeller blades so that even when the chord shrank to a line, the cavities were left behind the lifting lines. This portion

of cavity sheets was called "source sheets", the singularity strengths of which were obtained through the cavity sheet matching. This matching was totally different from the regular matching carried out for the properties belonging to the lifting line. It was considered that the present problem had to be categorized as the multiple scale problem in the singular perturbation method.

The first-order inner solution used a closure condition, i.e., the total source term S_0 equal to zero. It was considered that this assumption might not be totally correct, at least physically, because the cavity length was too long to be fully contained in the inner region. As the result of the cavity sheet matching, however, it was discovered that the second-order inner solution had to use a finite S_0 , the value of which was determined through the matching procedure. It seemed that the second-order matching automatically corrected the overstretching assumption made in the first-order inner solution.

In the section of problem classification, Section 3.0, two other problems were posed, both having small blade spacings. The outer solutions may be quite different from those in the above two cases since if one looks at such a propeller from the far field, the blade elements will not be identified. This may require the actuator disc concept for the outer solution, with a conventional pressure jump across the disc if the cavity is short but with a cavity pressure drop to be applied if the cavity is long, similar to the theory of Tulin (1965). These two problems have not been carried out here due to the enormous amount of work required even for the first two problems.

For the future study, therefore, the last two supercavitating problems having a large number of blades are recommended to be solved with the singular perturbation method. It is also our regret that numerical computations have not been conducted

for comparison of the present analytical results with experimental data for the same reason above. Such comparison will be interesting and is also recommended for further efforts.

REFERENCES

Abramowitz, M. and Stegun, I.A., 1964, Handbook of mathematical functions. National Bureau of Standards, U.S. Department of Commerce.

Bohn, J.C. and Altman, R., 1976, Two supercavitating propeller designs for hydrofoil ships. *Hydraulics Technical Report 7607, II-1*, May.

Bohn, J.C., 1977, Model tests of a supercavitating propeller designed for a hydrofoil ship. *Hydraulics Report 7607.59*, August.

Brockett, T., 1972, Propeller perturbation problems. *NSRDC, Report 3330*, October.

Cox, G.G., 1968, Supercavitating propeller theory - the derivation of induced velocity. *Seventh Symposium, Naval Hydrodynamics, August 25-30, Rome, Italy, sponsored by the Office of Naval Research, Department of the Navy*, pp. 329-349.

Erdelyi, A., Magnus, M., Oberhettinger, F. and Tricomi, F.G. (ed.), 1954, Tables of integral transforms. *Bateman Manuscript Project*, vol. 1, McGraw-Hill.

Fahner, J. and van Spiegel, E., 1966, Application of the method of singular integral equations to two-dimensional cavitating hydrofoil problems. *ASME publication 66-WA/FE-5*.

Furuya, O. and Acosta, A.J., 1973, A note on the calculation of supercavitating hydrofoils with rounded noses. *ASME Transactions, Journal of Fluids Engineering*, June, pp. 281-288.

Furuya, O., 1975, Three-dimensional theory on supercavitating hydrofoils near a free surface. *Journal of Fluid Mechanics*, vol. 71, part 3, pp. 589-609.

Furuya, O., 1976, Development of an off-design predictive method for supercavitating propeller performance. *Tetra Tech Report TC-676*, December.

Furuya, O., 1978, Theory improvement for computer code 'SCSCREW' prepared for DWTNSRDC. *Tetra Tech Report No. TC-3282*, December.

Furuya, O. and Maekawa, S., 1980, Study on a cavitating hydrofoil having a practical blade profile shape. *Tetra Tech Report No. TC-3284-07* prepared for the U.S. Navy under the GHR program.

James, E.C., 1975, Lifting-line theory for an unsteady wing as a singular perturbation problem. *Journal of Fluid Mechanics*, vol. 70, part 4, pp. 753-771.

Larock, R.E. and Street, R.L., 1965, A Riemann-Hilbert problem for nonlinear, fully cavitating flow. *Journal of Ship Research*, vol. 9, 170-173.

Larock, R.E. and Street, R.L., 1968, Cambered bodies in cavitating flow - a nonlinear analysis and design procedure. *Journal of Ship Research*, Vol. 12, 1-18.

Lechey, P., 1973, Supercavitating hydrofoils of finite span. *Proceedings of the IUTAM Symposium in Leningrad*, Nauka Publishing House, Moscow.

Muskhelishwili, N.I., 1946, Singular integral equations. *Noordhoff*, Gronigen, Holland.

Ogilvie, T.F., 1970, Singular perturbation problems in ship hydrodynamics. *Department of Naval Architecture and Marine Engineering, the University of Michigan*, Ann Arbor, Michigan.

Peck, J.G., 1977, Cavitation performance characteristics of supercavitating propellers 4698 and 4999. *CWTRNSRDC Ship Performance Department, Department Report SFD-680-02*, December.

Shen, Y.T. and Ogilvie, T.F., 1972, Nonlinear hydrodynamic theory for finite-span planing surface. *Journal of Ship Research*, 16, pp. 3-21.

Tulin, M.P., 1953, Steady two-dimensional cavity flows about slender bodies. *David Taylor Model Basin Rept. 334*, Washington, D.C.

Tulin, M.P., 1964, Supercavitating flows - small perturbation theory. *Journal of Ship Research*, vol. 7, no. 3.

Tulin, M.P., 1965, Supercavitating propellers - momentum theory. *Journal of Ship Research*, p. 158-169, December.

Van Dyke, M., 1964, Perturbation methods in fluid mechanics. *Academic*.

Wu, T.Y., 1962, A wake model for free streamline flow theory, Pt. I. Fully and partially developed wake flows and cavity flows past an oblique flat plate. *Journal of Fluid Mechanics* 18, 161-181.

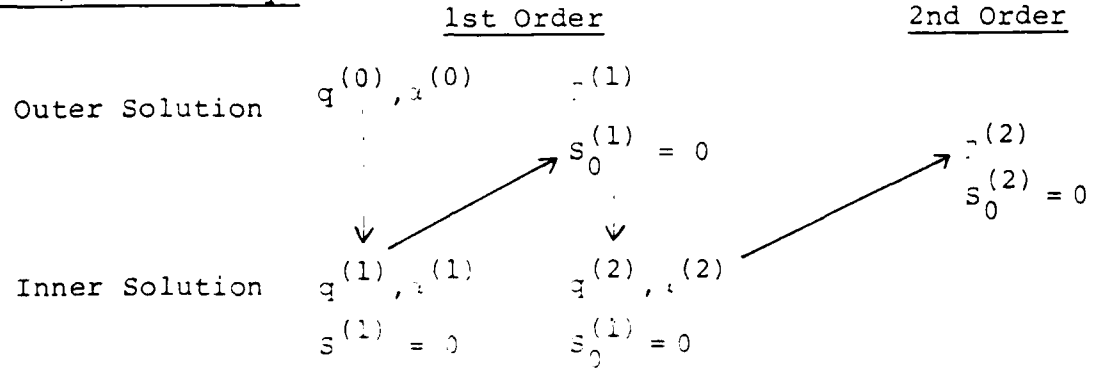
Yim, B.Y., 1978, A lifting surface theory of supercavitating propellers. *Joint Symposium on Design and Operation of Fluid Machinery*, ASME-IAHR/AIHR-ASME, held at Colorado State University, Fort Collins, Colorado, June 12-14, pp. 219-228.

TABLE 3.0.1
CLASSIFICATION OF S/C PROPELLER PROBLEMS IN SPM

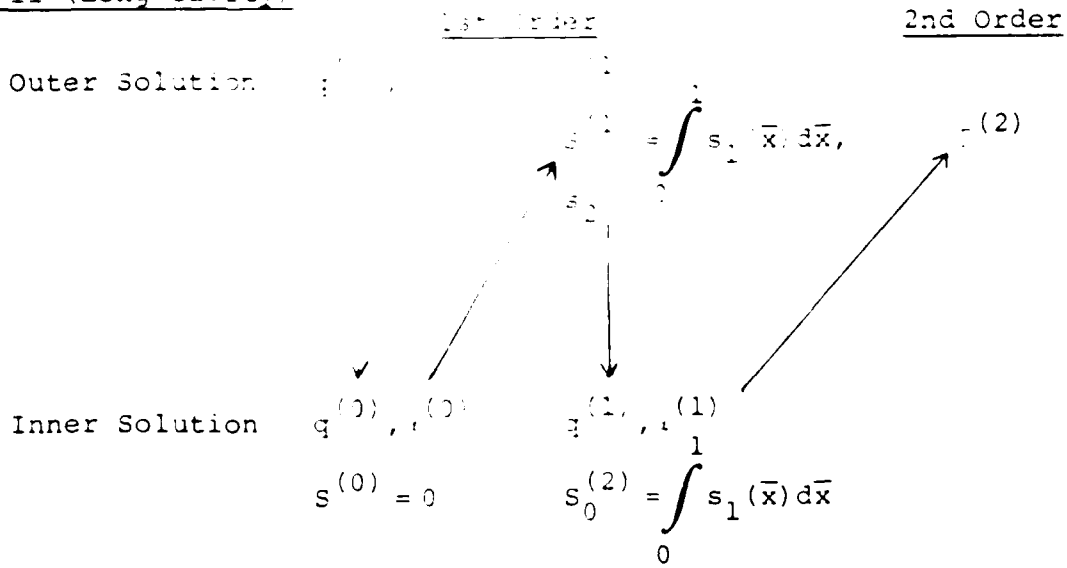
CASE NO.	SCALING	INNER SOLUTION	OUTER SOLUTION
I	$\frac{C}{R} = 0(\epsilon)$, $\frac{\lambda_C}{R} = 0(\epsilon)$ $\frac{d}{R} = 0(1)$	S/C single foil flow with a short cavity	Propeller lifting line theory
II	$\frac{C}{R} = 0(\epsilon)$, $\frac{\lambda_C}{R} = 0(1)$ $\frac{d}{R} = 0(1)$	S/C single foil flow with a long cavity	Propeller lifting line theory with source sheets behind blades
III	$\frac{C}{R} = 0(\epsilon)$, $\frac{\lambda_C}{R} = 0(\epsilon)$ $\frac{d}{R} = 0(1)$	S/C cascade flow with short cavities	Propeller actuator disk theory
IV	$\frac{C}{R} = 0(\epsilon)$, $\frac{\lambda_C}{R} = 0(1)$ $\frac{d}{R} = 0(\epsilon)$	S/C cascade flow with long cavities	Propeller actuator disk theory with source disk followed by source sheets

TABLE 3.2.1
MATCHING PROCEDURE AND RESULTS FOR CASE I AND CASE II

CASE I (Short Cavity)



CASE II (Long Cavity)



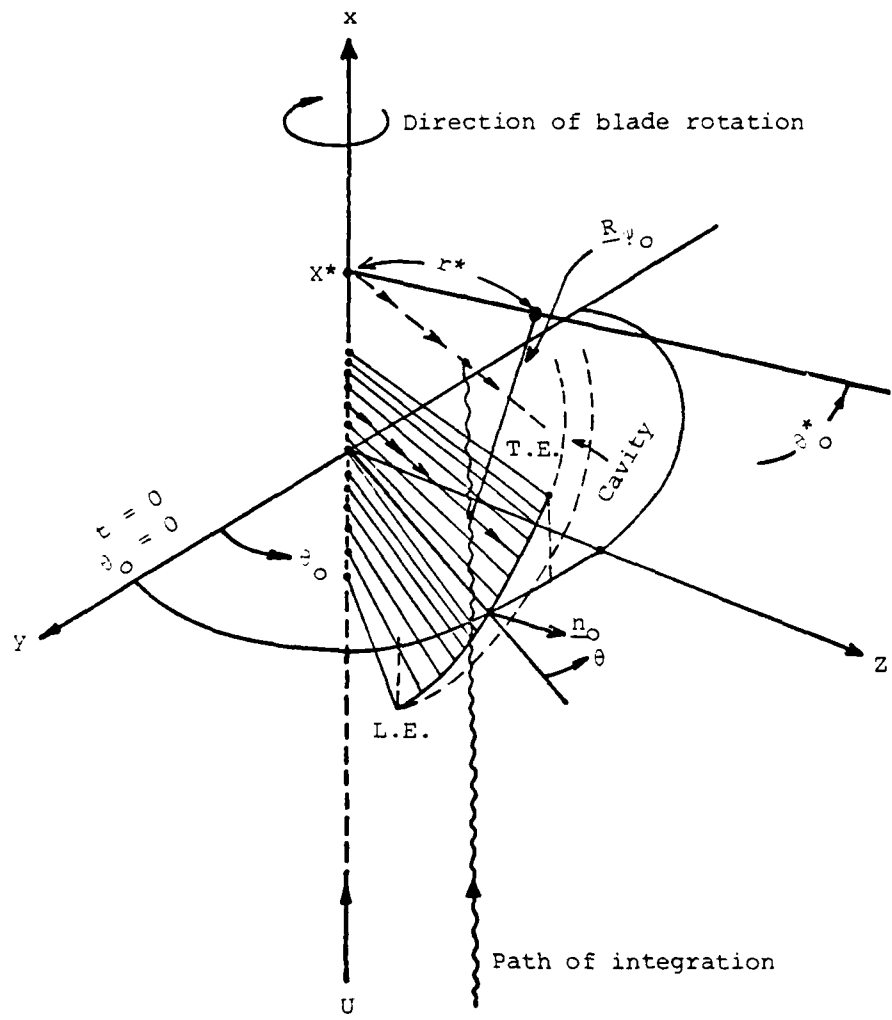
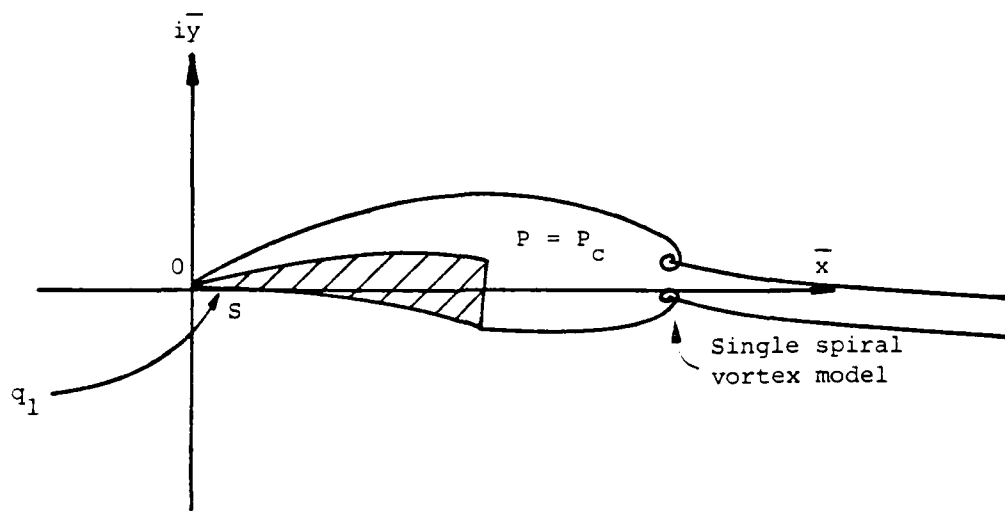
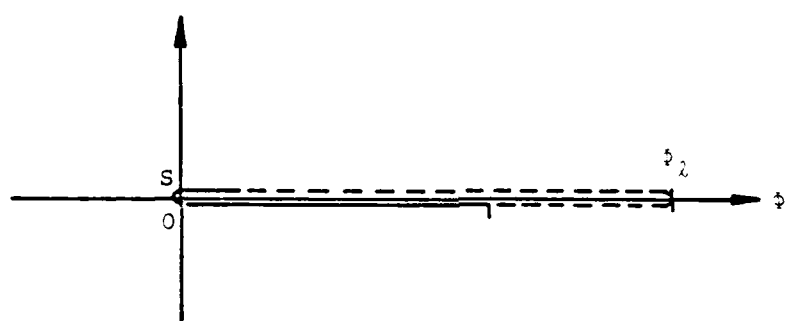


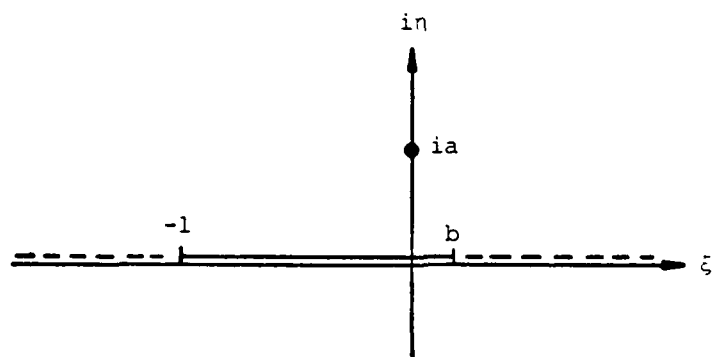
FIGURE 2.1.1 A schematic diagram for propeller flow configuration in which the propeller rotates at a fixed position while the flow approaches with the uniform velocity U



(a) Physical plane $\bar{\gamma} = \bar{x} = i\bar{y}$

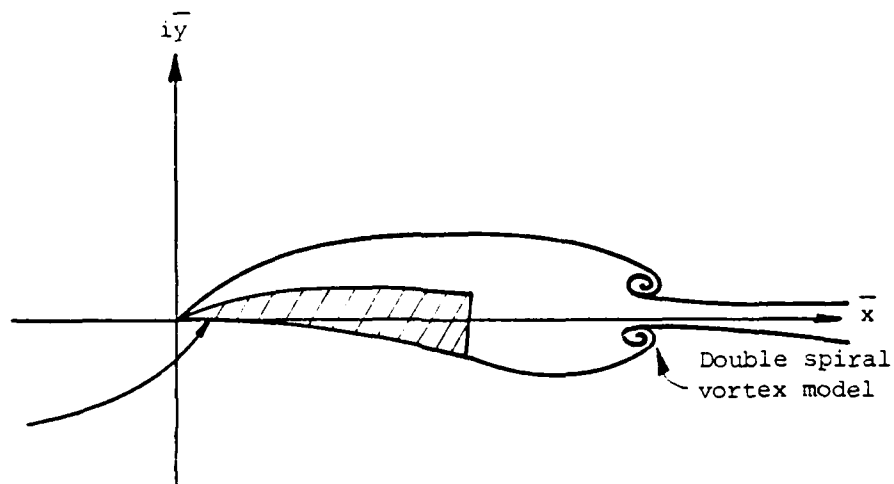


(b) Potential plane $W = \phi + i\psi$

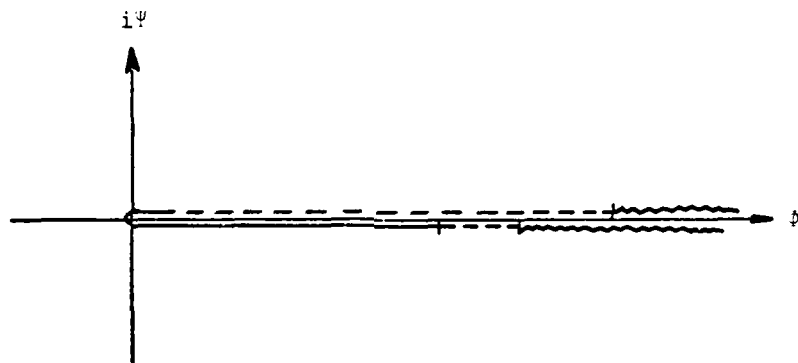


(c) Transform plane $\zeta = \xi + in$

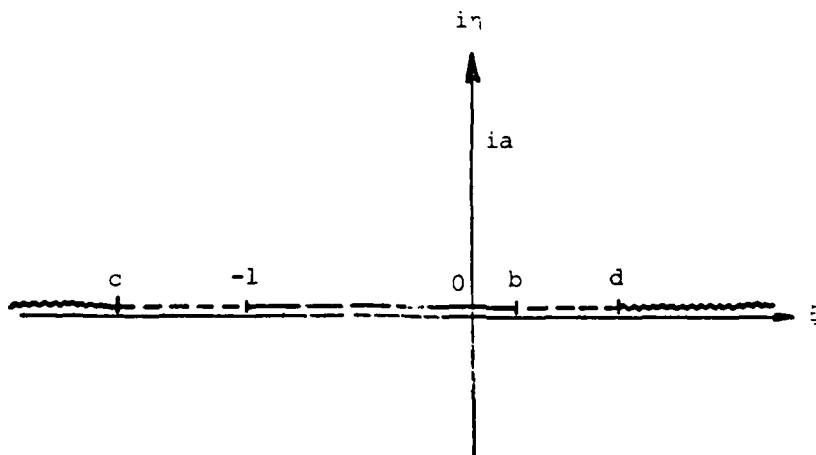
FIGURE 2.2.1 Flow configuration for a super-cavitating flow with single spiral vortex model in the physical plane and transform planes



(a) Physical plane $\bar{y} = \bar{x} + i\bar{y}$



(b) Potential plane $W = \phi + i\psi$



(c) Transform plane $\zeta = \xi + i\eta$

FIGURE 2.2.2 Flow configuration and transform planes for the same supercavitating flow as that in Figure 2.2.1 but with double spiral vortex model

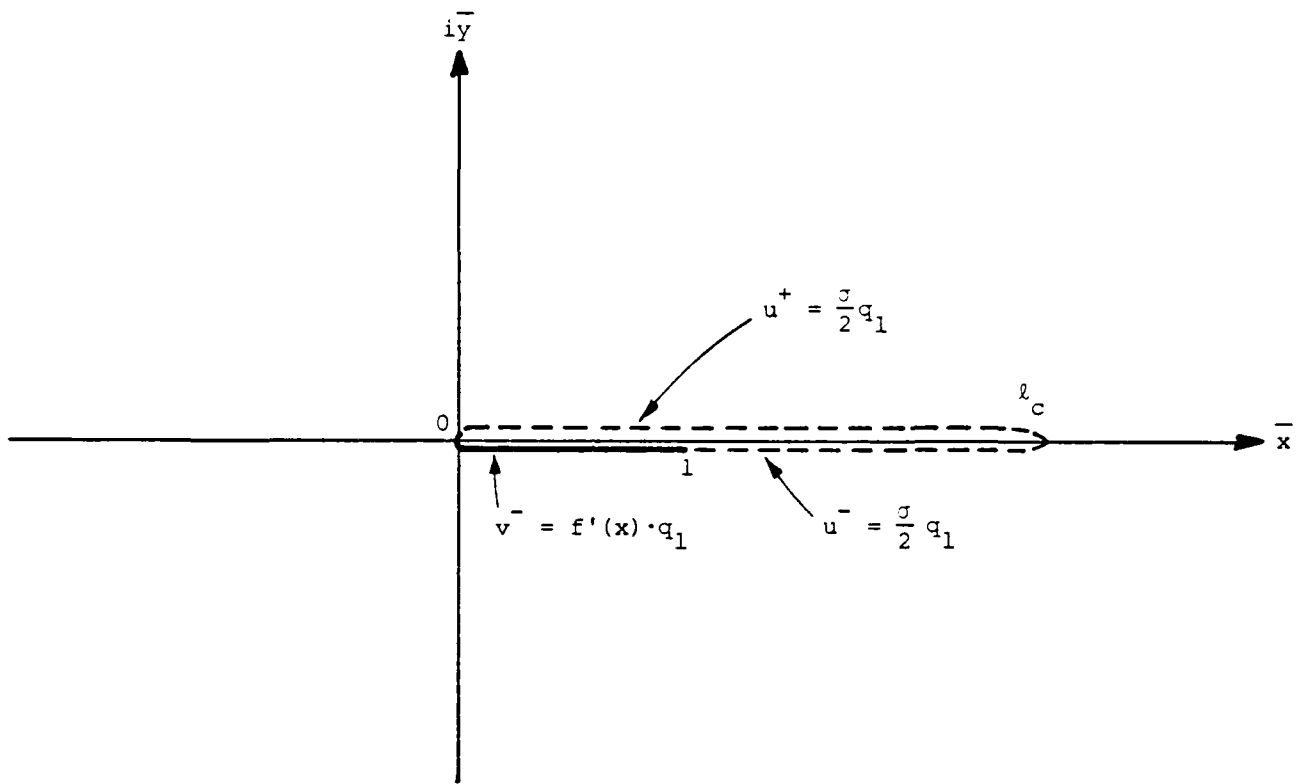
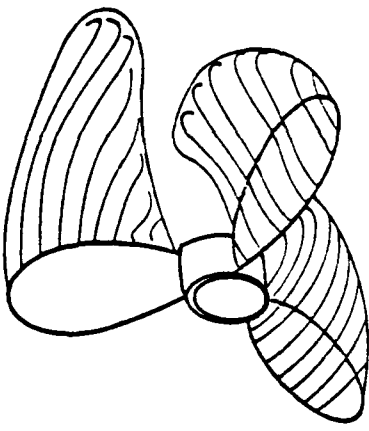
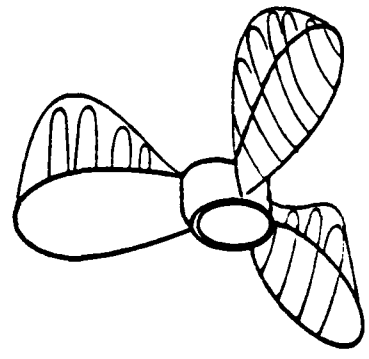


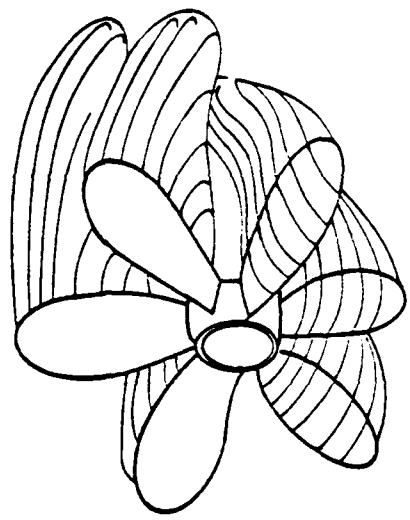
FIGURE 2.3.1 Linearized flow configuration for a supercavitating flow with boundary conditions



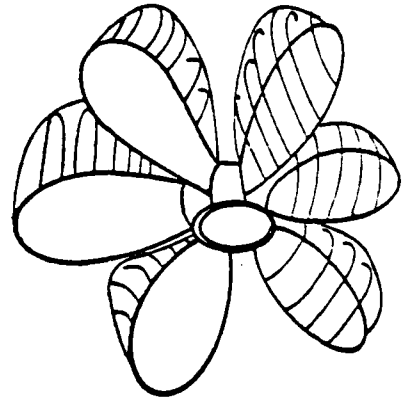
Case I: Short cavities
with a few blades



Case II: Long cavities
with a few blades



Case III: Short cavities
with many blades



Case IV: Long cavities
with many blades

FIGURE 3.0.1 Schematic flow configurations for various combinations of geometric and physical parameters (see Table 3.0.1 for detailed classifications)

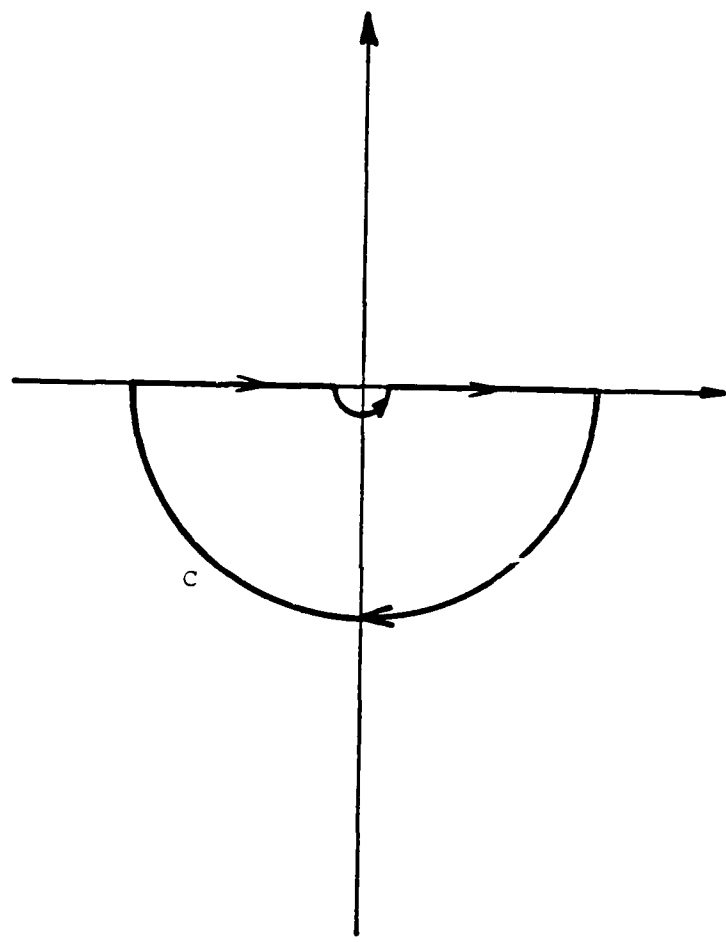


FIGURE 3.1.1 Contour C for the integral
of Equation (3.1.25)

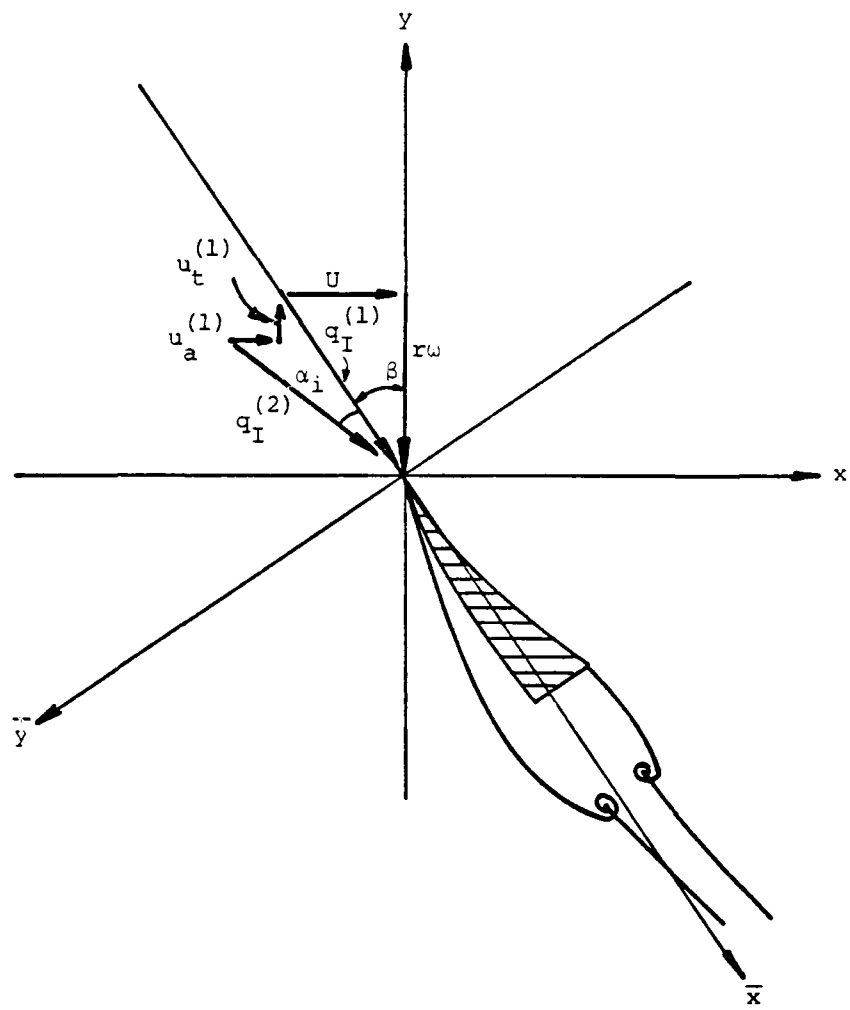
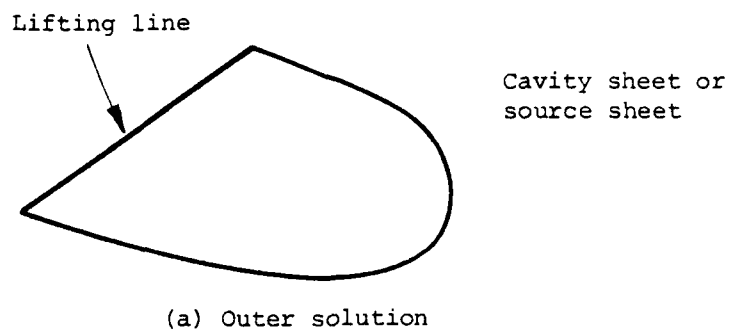
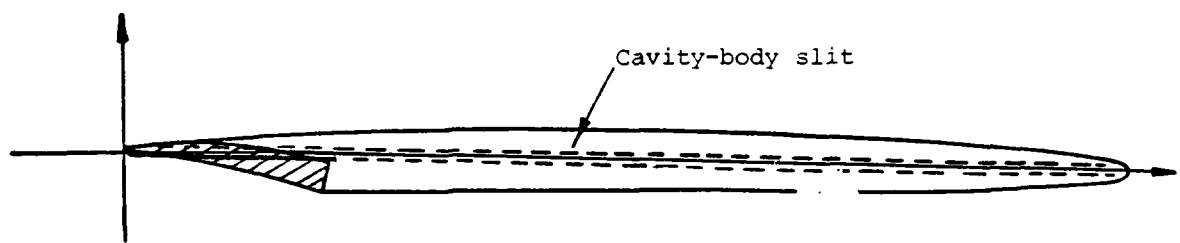


FIGURE 3.1.2 Local coordinate system (\bar{x}, \bar{y}) attached to the blade and incoming flow conditions



(a) Outer solution



(b) Inner solution

FIGURE 3.2.1 Flow configuration for (a) the outer and (b) inner solutions in Case II

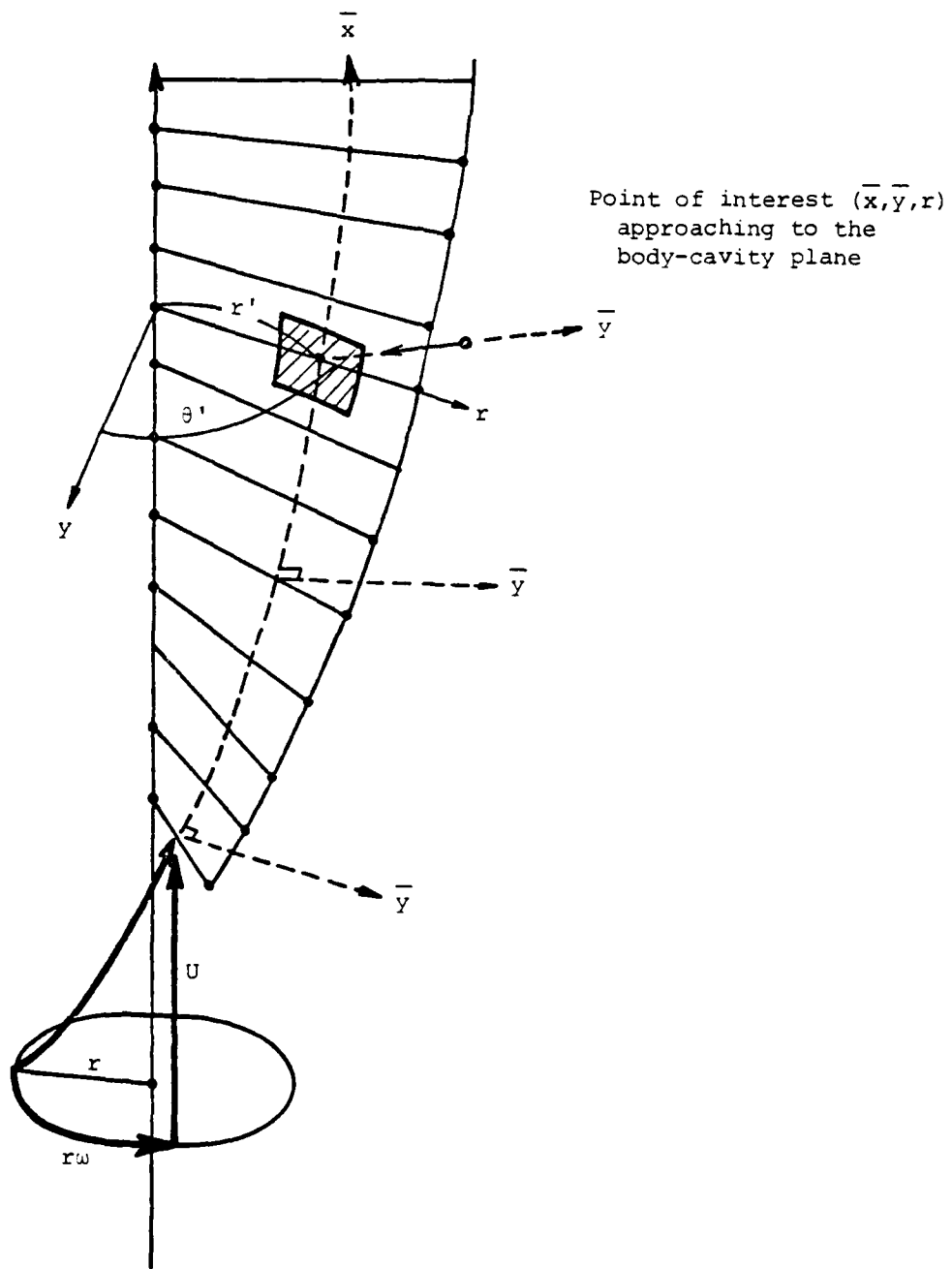


FIGURE 3.2.2 Expansion of the source singularity around the local coordinate system (\bar{x}, \bar{y}, r)

APPENDIX A
INVERSION FORMULA OF SINGULAR INTEGRAL EQUATIONS

The inversion formula of the singular integral equation for arcs is well described in the book of Muskhelishvili (1946). In order to provide a brief insight into the derivation of the formula the inversion method will be summarized herein. Let the singular integral equation be defined by

$$\frac{1}{\pi i} \int_L \frac{\phi(t) dt}{t - t_0} = f(t_0) \text{ on } L \quad (A-1)$$

where the contour L consists of smooth arcs L_1 to L_p , i.e.,

$$L = L_1 + L_2 + \cdots + L_p, \quad (A-2)$$

$f(t)$ is a given function and $\phi(t)$ is to be determined. The functions $f(t)$ and $\phi(t)$ are considered to belong to the classes H^1 ¹⁾ and H^* ²⁾, respectively.

Note: 1) A function $\phi(t)$ will be said to satisfy a Hölder condition (or H condition) on the arc L , if for any two points t_1, t_2 of L

$$|\phi(t_2) - \phi(t_1)| \leq A |t_2 - t_1|^\mu$$

where A and μ are positive constants. The function $\phi(t)$ will be said to belong to the class H on L , if it satisfies the $H(\mu)$ condition for some $\mu > 0$ on each of the closed arcs L_j of L including the ends.

2) If the function $\phi(t)$, given on L , satisfies the $H(\mu)$ condition on every closed part of L not containing ends, and if near any end c it is of the form

$$\phi(t) = \frac{\phi^*(t)}{(t - c)^\alpha} \quad 0 \leq \alpha < 1$$

where $\phi^*(t)$ belongs to the class H , then $\phi(t)$ will be said to belong to the class H^* on L .

Introducing a sectionally holomorphic function

$$\phi(z) = \frac{1}{2\pi i} \int_L \frac{\phi(t) dt}{t - z}, \quad (A-3)$$

one has

$$\phi^+(t_0) + \phi^-(t_0) = \frac{1}{\pi i} \int_L \frac{\phi(t) dt}{t - t_0}.$$

Therefore, the inversion of the singular integral equation (A-1) is equivalent to the problem

$$\phi^+(t_0) + \phi^-(t_0) = f(t_0) \text{ on } L, \text{ and} \quad (A-4)$$

$$\phi(\infty) = 0.$$

This is a well-known mixed-type boundary value problem, the solution method for which requires first the homogeneous solution $x(z)$ of $\phi^+(t_0) + \phi^-(t_0) = 0$. By choosing a function

$$x(z) = \left\{ \frac{R_1(z)}{R_2(z)} \right\}^{\frac{1}{2}} \quad (A-5)$$

where

$$R_1(z) = \prod_{k=1}^q (z - c_k) \quad (A-6)$$

$$R_2(z) = \prod_{k=q+1}^{2p} (z - c_k) \quad (A-7)$$

and the quantity of $x(z)$ is understood to refer to the branch cut along L . It is readily found then that

$$[x(z)]^+ = - [x(z)]^- \quad (A-8)$$

and therefore a solution to the problem for a new function $y(z)$

$$y(z) = \frac{\phi(z)}{x(z)} \quad (A-9)$$

is given by solving a boundary value problem

$$\begin{aligned} Y^+ - Y^- &= \left[\frac{\phi(z)}{X(z)} \right]^+ - \left[\frac{\phi(z)}{X(z)} \right]^- = \frac{[\phi(z)]^+ + [\phi(z)]^-}{[X(z)]^+} \\ &= \frac{f(t)}{[X(t)]^+} \quad \text{on } L \end{aligned} \quad (A-10)$$

The solution for $Y(z)$ is given

$$Y(z) = \frac{1}{2\pi i} \int_L \frac{f(t)}{[X(t)]^+} \frac{dt}{t - z} + Q(z) \quad (A-11)$$

where $Q(z)$ is an arbitrary polynomial. The solution for $\phi(z)$ is therefore obtained by substituting (A-11) into (A-9),

$$\phi(z) = X(z) \left[\frac{1}{2\pi i} \int_L \frac{f(t)}{[X(t)]^+} \frac{dt}{t - z} + Q(z) \right]. \quad (A-12)$$

The arbitrary polynomial $Q(z)$ will be chosen in such a way that $\phi(\infty) = 0$ and other physical conditions of the problem such as singularities be satisfied.

